PHYSICAL REVIEW D **96,** 015026 (2017)

Searching for signatures of E_6

Aniket Joglekar and Jonathan L. Rosner
Enrico Fermi Institute and Department of Physics, University of Chicago, Chicago, Illinois 60637, USA
(Received 29 November 2016; published 24 July 2017)

The grand unified group E_6 is a predictive scheme for physics beyond the standard model (SM). It offers the possibility of extra Z bosons, new vectorlike fermions, sterile neutrinos, and neutral scalars in addition to the SM Higgs boson. Some previous discussions of these features are updated and extended. Their relevance to present searches at the CERN Large Hadron Collider and in patterns of neutrino masses is noted. Addition of a small set of scalar bosons at the TeV scale permits gauge unification near a scale of 10^{16} GeV and leads to bounds on masses of particles beyond those in the standard model.

DOI: 10.1103/PhysRevD.96.015026

I. INTRODUCTION

Candidates for unification of the standard model (SM) electroweak and strong interactions include the groups SU(5) [1], SO(10) [2,3], and E_6 [4]. The known left-handed quarks and leptons may be accommodated in three $\bar{5} + 10 + 1$ reducible representations of SU(5). The singlets correspond to left-handed weak isosinglet antineutrinos, needed to accommodate neutrino oscillations. SO(10) unifies the representations in each family into three 16-dimensional spinors, with the "seesaw" mechanism a popular way to understand the smallness of neutrino masses [5]. Each 27-dimensional fundamental representation of E_6 contains not only a 16-plet spinor of SO(10), but an SO(10) 10-plet vector and an SO(10) singlet:

$$27 = 16 + 10 + 1. \tag{1}$$

The 10-plet of SO(10) contains a $5 + \bar{5}$ of SU(5), where the $\bar{5}$ contains an electroweak singlet color-antitriplet antiquark D^c with charge $1/3$ and an electroweak lepton doublet (L^-, L^0). The pairing of $\bar{5}$ with 5 implies that the couplings of electroweak gauge bosons to members of the SO(10) 10-plet are purely vectorlike, with no axial-vector component. The singlet n of SO(10) has no tree-level coupling to gluons or electroweak gauge bosons, aside from that induced by mixing with other neutral leptons.

Signatures of E_6 include extension of the Higgs sector [6]; existence of neutral Z' gauge bosons at masses above the electroweak scale whose decays in hadronic collisions display characteristic forward-backward asymmetries [7–10]; the production of new vectorlike quarks and leptons [11–13]; and manifestations of the neutral fermion n through its mixing with other neutral leptons, giving rise to signatures of "sterile" neutrinos [10,14–24]. Up to now, with the possible exception of weak evidence for sterile neutrinos [25–34] there has been no indication of the extra degrees of freedom entailed by the 27-plet of E_6.

A potential change in this situation occurred with claims by the ATLAS [35,36] and CMS [37,38] Collaborations at the CERN Large Hadron Collider (LHC) of a diphoton enhancement around 750 GeV. The accumulation of further data by both collaborations did not confirm this effect, which now appears to have been a statistical fluctuation [39–41]. Nonetheless, great interest was stirred in the theoretical community, leading to reexamination of predictions of many existing schemes and invention of new ones. In the present paper, we pursue one such avenue, updating and extending some previous investigations of E_6.

Other recent discussions of E_6 stimulated by the initial CERN digamma reports but with more general validity include those in [42–56]. See also extensive earlier work on E_6 in Refs. [57–79]. Early phenomenological analyses include ones by [80–83]. For a critical review of more than 200 papers on the initial hints of a signal see [84], with Ref. [85] proposing a number of future experiments to pin down related physics. Some treatments incorporated key elements (such as vectorlike fermions) of E_6 without citing it: e.g., [86–90]. (The introduction of heavy vectorlike fermions avoids large contributions to the S parameter of Peskin and Takeuchi [91–93].) Subgroups of E_6 other than $SU(5) \otimes U(1)_\psi \otimes U(1)_\chi$, including $SU(3)_c \otimes SU(3)_L \otimes SU(3)_R$ and various forms of $SU(6) \otimes SU(2)$ [8,9,94–96], have been used by many authors in variants of the present scheme.

As in Refs. [14,15,97–100], we shall assume fermion masses arise from a coupling of two 27-plet fermions with a 27-plet scalar multiplet. We shall label all members of this multiplet with a tilde, without assuming that they are supersymmetric partners of the corresponding fermions. In particular, a scalar state $\tilde{n}$ should exist as a counterpart to the neutral fermion n described above. While it was tempting to associate it with the effect at 750 GeV, its properties remain of interest even if it has not yet been observed. Our main focus will be to develop guidance for experimental searches that could confirm or disprove the E_6 picture at the TeV scale.

The E_6 symmetry is considered to be spontaneously broken at the grand unified theory (GUT) scale, first to

$SO(10) \otimes U(1)_\psi$, which is then broken to $SU(5) \otimes U(1)_\psi \otimes U(1)_\chi \to SU(5) \otimes U(1)_N$ at the same scale. [$U(1)_N$ is that linear combination of $U(1)_\psi$ and $U(1)_\chi$ for which the left-handed antineutrino has zero charge. For a recent model incorporating it, see Ref. [56].] To achieve this breaking, in addition to the 27-plet scalar generation, we also must have a 78-plet of E_6. Three SM singlets in the 78-plet—one is a singlet under SO(10), another is a singlet under the SU(5) contained in 45 of SO(10) and the third one is a singlet under the SM gauge group contained in 24 of SU(5) in 45 of SO(10)—acquire vacuum expectation values (VEVs) of the order of the GUT scale, facilitating the spontaneous symmetry breaking of E_6 down to the SM gauge group. Details are described in the next section.

Our model also has a 351′-plet scalar [101] that contains scalar diquarks, an SU(2) triplet, and an SU(3) octet with appropriate $U(1)_N$ charges (see Table XI in Appendix A) preventing them from contributing to proton decay. Such particles then can exist at the TeV scale, helping to achieve unification of the SM gauge couplings and raising the unification scale to avoid violating current bounds on proton decay processes.

In Sec. II we decompose a 27-plet of E_6 into its SO(10) and SU(5) components, with U(1) subgroups arising from $E_6 \to SO(10) \otimes U(1)_\psi$ and $SO(10) \to SU(5) \otimes U(1)_\chi$ [8,9]. The corresponding neutral gauge bosons are denoted Z_ψ and Z_χ, respectively. We adopt a linear combination of $U(1)_\psi$ and $U(1)_\chi$ [102,103] under which the right-hand neutrino has zero charge, allowing it to have a large Majorana mass through a higher-dimension operator [20,70,104]. The gauge boson coupling to this $U(1)_N$ charge will be denoted Z_N. We also explain the details of symmetry breaking due to the 78-plet and unification due to low-energy components of the 351′-plet. (Reference [105] contains useful group-theoretic results.) We then enumerate E_6-invariant couplings in Sec. III.

Under general circumstances a $\tilde{n}$ can mix with the Higgs boson. A general discussion of potentials and mass matrices for (pseudo)scalars, in Sec. IV, indicates conditions under which this mixing can be suppressed to acceptable levels. The renormalization-group evolution of gauge and Yukawa couplings, important because of the need to avoid Landau singularities, is discussed in Sec. V. Production and decays of $\tilde{n}$ are mediated by loops of exotic fermions in the SO(10) 10-plets belonging to the E_6 27-plet. We discuss the decays of $\tilde{n}$ to $\gamma\gamma$, γZ, ZZ, and W^+W^- in this picture in Sec. VI. Section VII treats cross sections for $\tilde{n}$ production and observation in the $\gamma\gamma$ mode.

The properties of the heavy vectorlike leptons L and weak isosinglet quarks D belonging to the SO(10) 10-plet depend on their decay schemes. We shall adopt a $\mathbb{Z}_2$ symmetry [15] under which SO(10) 16-plets are odd while 10-plets and singlets are even. This opens the possibility of stable neutral scalars or fermions which could be dark matter candidates. The neutral lepton states n and neutrino mixing schemes involving them, discussed in Ref. [15], are updated under the assumption of an exact $\mathbb{Z}_2$ symmetry in Sec. VIII, where we also remark briefly on the consequences of this symmetry for dark matter.

We estimate cross sections and signatures for the heavy fermions in the SO(10) 10-plet in Sec. IX and suggest diagnostics for extra neutral gauge bosons such as Z_N in Sec. X. In Sec. XI, we bring together the constraints on the various types of exotic particles to show how tightly constrained the mass spectrum is. We use these constraints to make future projections for the confirmation or exclusion of the model. We conclude in Sec. XII. Appendix A describes the details of ψ, χ and N charges of the SU(5) components of the scalar sector. Appendix B treats details of potentials for scalar and pseudoscalar mesons, while Appendix C is devoted to particulars of the renormalization group evolution.

II. U(1) CHARGES AND MULTIPLET MEMBERS

A. Fermions

Under the decomposition $E_6 \to SO(10) \otimes U(1)_\psi \to SU(5) \otimes U(1)_\psi \otimes U(1)_\chi$, a fermion 27-plet decomposes as shown in Table I. The charge

$$Q_N = -\frac{\sqrt{15}}{4} Q_\psi - \frac{1}{4} Q_\chi \tag{2}$$

TABLE I. Left-handed fermions in the 27-plet of E_6, their SO(10) and SU(5) representations, and their U(1) charges. Subscripts $i = 1, 2, 3$ on the fermions denote family: $d_{1,2,3} = (d, s, b)$; $u_{1,2,3} = (u, c, t)$; $e_{1,2,3} = (e, \mu, \tau)$.

SO(10), SU(5)	$2\sqrt{6}Q_\psi$	$2\sqrt{10}Q_\chi$	$2\sqrt{10}Q_N$	Fermion	$SU(3)_c$	Q
$16, \bar{5}$	1	3	−2	d_i^c	$\bar{3}$	1/3
				ν_i	1	0
				e_i^-	1	−1
16, 10		−1	−1	u_i	3	2/3
				d_i	3	−1/3
				u_i^c	$\bar{3}$	−2/3
				e_i^+	1	1
16, 1		−5	0	N_i^c	1	0
$10, \bar{5}$	−2	−2	3	D_i^c	$\bar{3}$	1/3
				L_{1i}^0	1	0
				L_{1i}^-	1	−1
10, 5		2	2	D_i	3	−1/3
				L_{2i}^+	1	1
				L_{2i}^{0c}	1	0
1, 1	4	0	−5	n_i	1	0

is that linear combination of Q_ψ and Q_χ for which the left-handed antineutrinos N_i^c are neutral, allowing them to obtain large Majorana masses via higher-dimension operators. We use the notation of Ref. [9] except that in accord with common use today, exotic isovector leptons are labeled here as L_i, with $i = 1, 2, 3$ denoting family, and isosinglet heavy quarks with charge $-1/3$, called h_i in the 1980s, are labeled here as D_i in order to avoid confusion with the Higgs boson. (We will not be discussing charmed mesons, elsewhere called D, in this paper.)

B. Scalars

Whereas we assumed three families of 27-plet fermions, we consider only a single 27-plet of scalar bosons, whose neutral members are allowed to obtain nonzero VEVs. These are listed in Table II. We have adopted a tilde to denote the spin-zero partner of the corresponding fermion first family. This is in contrast to exceptional supersymmetric models [57–72] in which three 27-plets of fermions are accompanied by three 27-plets of (pseudo)scalars.

We shall discuss trilinear fermion-fermion-scalar couplings systematically in the next section. Meanwhile we describe the roles of VEVs of each of the five scalars in a 27-plet. We list the left-handed fermion pairs which form an E_6 singlet when coupled to each scalar. We ignore for now interfamily mixing in quarks and leptons. The numbers after each scalar denote values of $(2\sqrt{6}Q_\psi, 2\sqrt{10}Q_\chi, 2\sqrt{10}Q_N)$. More details about the effects of each VEV on neutral lepton spectra are given in Ref. [15]. There, a $\mathbb{Z}_2$ symmetry was imposed whereby 16-plet VEVs (with $\mathbb{Z}_2$ quantum number -1) were suppressed in comparison with 10-plet and singlet VEVs (with $\mathbb{Z}_2$ quantum number 1). Thus,

$$\langle\tilde{\nu}\rangle, \langle\tilde{N}\rangle \ll \langle\tilde{L}_1^0\rangle, \langle\tilde{L}_2^{0c}\rangle, \langle\tilde{n}\rangle. \tag{3}$$

Presently we shall compare decay schemes of 10-plet fermions in cases where this $\mathbb{Z}_2$ is exact with ones where it is approximate. A very recent work [106] also makes use of this $\mathbb{Z}_2$.

TABLE II. Scalar mesons in a 27-plet of E_6, their SO(10) and SU(5) representations, and their U(1) charges.

SO(10), SU(5)	$2\sqrt{6}Q_\psi$	$2\sqrt{10}Q_\chi$	$2\sqrt{10}Q_N$	Meson	$SU(3)_c$	Q
$16, \bar{5}$	1	3	−2	$\tilde{d}^c$	$\bar{3}$	1/3
				$\tilde{\nu}_e$	1	0
				$\tilde{e}^-$	1	−1
16, 10		−1	−1	$\tilde{u}$	3	2/3
				$\tilde{d}$	3	−1/3
				$\tilde{u}^c$	$\bar{3}$	−2/3
				$\tilde{e}^+$	1	1
16, 1		−5	0	$\tilde{N}^c$	1	0
$10, \bar{5}$	−2	−2	3	$\tilde{D}^c$	$\bar{3}$	1/3
				$\tilde{L}_1^0$	1	0
				$\tilde{L}_1^-$	1	−1
10, 5		2	2	$\tilde{D}$	3	−1/3
				$\tilde{L}_2^+$	1	1
				$\tilde{L}_2^{0c}$	1	0
1, 1	4	0	−5	$\tilde{n}$	1	0

Neutral scalar bosons in E_6, their SM $\otimes$ $U(1)_N$-invariant couplings to left-handed fermion pairs, and the effects of their VEVs (family indices omitted for simplicity) are as follows:

(i) $\tilde{\nu}(1, 3, -2)$: $(e^+L_1^-), (dD^c), (N^cL_2^{0c})$: Mixes e and L, d and D; VEV small. Exchange can contribute to exotic fermion pair production, e.g., in the reaction $e^+e^- \to L^+L^-$ or $dd^c \to DD^c$.

(ii) $\tilde{N}^c(1, -5, 0)$: $(d^cD), (e^-L^+), (\nu L_2^{0c}), (N^cN^c)$: Mixes e and L, d and D; VEV small. Provides a small Majorana mass contribution to N^c, which obtains most of its Majorana mass from a higher-dimension operator. Exchange can contribute to exotic fermion pair production, e.g., in the reaction $e^+e^- \to L^+L^-$ or $dd^c \to DD^c$.

(iii) $\tilde{L}_1^0(-2, -2, 3)$: $(L_2^{0c}n), (dd^c), (e^+e^-)$: Dirac masses for down-type quarks, charged SM leptons. Its VEV is v_d in the standard two-Higgs-doublet model.

(iv) $L_2^{0c}(-2, 2, 2)$: $(L_1^0n), (\nu N^c), (uu^c)$: Dirac masses for neutrinos (overwhelmed by seesaw), up-type quarks. Its VEV is v_u in the standard two-Higgs-doublet model.

(v) $\tilde{n}(4, 0, -5)$: $(L_1^0L_2^{0c}), (L_2^+L_1^-), (DD^c)$: Dirac masses for SO(10) fermionic 10-plet members.

As explained in Appendix A, the scalar 78-plet contains five singlets under the SM gauge symmetry. The 78 (adjoint representation) of E_6 decomposes under SO(10) as follows:

$$78 = 1 + 45 + 16 + \overline{16}. \tag{4}$$

The first component, which is a singlet under SO(10), can acquire a GUT-scale VEV to break $E_6 \to SO(10) \otimes U(1)_\psi$. The 45 of SO(10) then can be decomposed into SU(5) representations as

$$45 = 1 + 24 + 10 + \overline{10}. \tag{5}$$

The first component, which is a singlet under SU(5), can acquire a GUT-scale VEV to break $SO(10) \to SU(5) \otimes U(1)_\chi$. Now the 24 of SU(5) contains a singlet under the SM gauge group which can also acquire a GUT-scale VEV that breaks SU(5) to the SM. There is also the breaking $U(1)_\psi \otimes U(1)_\chi \to U(1)_N$ which is driven by a 351′-plet VEV as described below. Thus the symmetry surviving from the GUT scale down to the TeV scale is SM $\otimes$ $U(1)_N$. At the TeV scale $U(1)_N$ is broken due to the VEV of another

singlet contained in the 351′-plet that gives a Z_N boson its mass. There are two other singlets under $SU(5)$ contained in the 78-plet which have nonzero $U(1)_N$ charge (see Table VIII in Appendix A). Thus in the interest of preserving $U(1)_N$ charges down to the TeV scale in order to preserve the other desired properties of the model including the low-energy diquarks that unify the gauge couplings, we do not give VEVs to these. They have terms arising from the VEVs of the other 78-plet singlets which give rise to masses at the GUT scale. Thus, all of the scalar 78-plet resides at the GUT scale.

The scalar 351′-plet decomposes under SO(10) [105] as

$$351' = 1 + 10 + \overline{16} + 54 + \overline{126} + 144. \tag{6}$$

The first component [a nonsinglet of $U(1)_N$] eventually acquires a VEV at the TeV scale that gives mass to the Z_N boson. A lower bound on this VEV is set by the maximum value of g_N allowed by the unification and the experimental search lower bounds on Z'_N boson masses [107–112]. More details of this are discussed in Sec. X. The $\overline{126}$ above, when decomposed under SU(5), also contains a singlet which has nonzero Q_ψ and Q_χ charges but no Q_N charge. Thus it is the one which acquires a GUT-scale VEV to break $U(1)_\psi \otimes U(1)_\chi$ to $U(1)_N$.

Finally, the unification of the SM gauge couplings at a satisfactorily high scale requires new particles at TeV scales carrying more SU(2) and SU(3) charges than their $U(1)_Y$ charges. This will modify their beta functions so as to prevent their coupling constants from unifying with $U(1)_Y$ at energies forbidden by proton decay bounds. Diquarks, an SU(2) triplet, and an SU(3) color octet are suitable candidates for this. The difference in magnitude of Abelian and non-Abelian charges carried by diquarks is larger than that of any other type of fermions. The presence of the triplet and octet helps to adjust the beta functions without touching the $U(1)_Y$ beta function, thereby letting the GUT scale be set above the bound from $p \to e^+\pi^0$ [113].

The new particles need to be at the multi-TeV (MTeV) scale in order to achieve unification. Their potential role as mediators of proton decay can be avoided if they have $U(1)_N$ charges of magnitude $\pm 5/\sqrt{40}$ or larger. They then cannot couple to pairs of SM fermions, whose total Q_N charges are never greater in magnitude than $\pm 4/\sqrt{40}$.

The 351′-plet contains particles which exactly possess all these properties with Q_N charges of $\pm 6/\sqrt{40}$ for diquarks and $-5/\sqrt{40}$ for the triplet and the octet. Details are given in Appendix A, Table XI. Such high charges forbid tree-level couplings with two quarks or with a quark and a lepton which could have facilitated proton decay. This is because all the SM particles carry Q_N charges no larger than $\pm 2/\sqrt{40}$. The SO(10) singlet with Q_N charge of $10/\sqrt{40}$ is chosen to be at MTeV scale in order to be able to break $U(1)_N$ symmetry at that scale to give mass to the Z_N boson.

Loop-induced couplings of these TeV-scale states to two quarks or a quark and a lepton are possible. But the coupling to two quarks is heavily suppressed by the presence of the colored scalar quarks belonging to the 27-plet, as shown in Fig. 1, which have GUT-scale masses as discussed in the next section. Couplings to a quark and a lepton can involve exotic fermions and scalar neutrinos belonging to 27-plets so they are not as heavily suppressed as couplings to two quarks, but nonetheless proton decay is forbidden as it requires both types of couplings. Other potentially dangerous operators listed in [114] are also forbidden mainly owing to the high values of Q_N charges that these new particles carry.

The diquark states that belong to 15 of SU(5) contained in 54 of SO(10) and $\overline{10}$ of SU(5) contained in $\overline{16}$ of SO(10) (see Table XI in Appendix A) have mass bounds due to leptoquark and dijet searches [115–119]. We do not perform any explicit analysis of these, but we avoid these bounds by assuming these diquark states to be above a few TeV. The rich phenomenology of this sector is beyond the scope of the present work. Details of the unification can be found in Appendix C. Thus, the 351′-plet plays an important role in the symmetry breaking, Z_N mass, and nonsupersymmetric unification of SM gauge couplings in the present model.

It is important to note that the 351′-plet has the same splitting problem as the doublet-triplet splitting in the

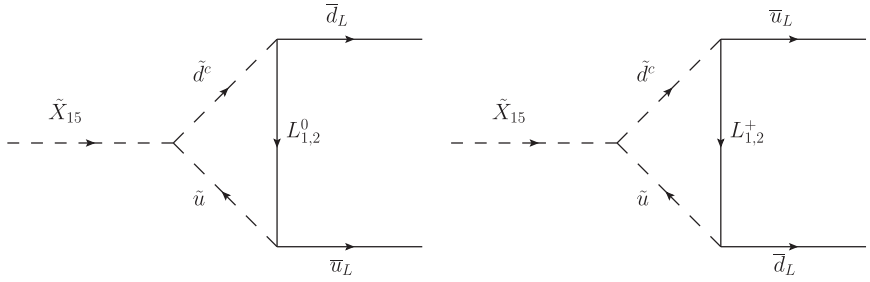

FIG. 1. $\tilde{X}_{15}$ is a diquark belonging to the 15 of SU(5) in the 54 of SO(10) contained in the scalar 351′ of E_6, which couples to two SM quarks at one-loop level. The loop involves particles with GUT-scale masses and therefore is suppressed. Another multi-TeV-scale diquark, $\tilde{X}_{10}$ (not shown) belongs to the $\overline{10}$ of SU(5) in the $\overline{16}$ of SO(10) contained in the scalar 351′ of E_6. It does not couple to two SM quarks at the one-loop level. For quantum numbers of $\tilde{X}_{15}$ and $\tilde{X}_{10}$ see Table XI.

27-plet, as some of its components reside at the GUT scale while others reside at the TeV scale (see the mass scale column of Table XI in Appendix A). We assume that the model can be fine-tuned to achieve such a large splitting owing to the large number of parameters in the potential. The scalar 78-plet does not suffer from this problem as it all resides at the GUT scale.

In summary, E_6 is broken to SM $\otimes$ $U(1)_N$ at the GUT scale. Then $U(1)_N$ is broken at the TeV scale and SU(2) at the electroweak scale. At the TeV scale or below, our model has SM gauge bosons, SM and exotic fermions; and scalars consisting of colorless weak doublets and $\tilde{n}$ in the 27-plet, and diquarks, SU(2) triplet, SU(3) color octet, and a $U(1)_N$-breaking SO(10) singlet in a $351'$-plet. This gives rise to the interesting phenomenology discussed below and achieves one-loop unification (Appendix C).

III. INVARIANT COUPLINGS

We now list the *charged* scalars permitted to couple to left-handed fermion pairs by invariance under the SM $\otimes$ $U(1)_N$. Some of these couplings will lead to proton instability unless the corresponding scalars are very massive. This is the famous doublet-triplet splitting problem (see [120]; see also [121,122], and references therein). For convenience we omit family indices on fermions.

(i) $\tilde{d}^c(1,3,-2)$: $(dL_1^0),(uL_1^-),(N^cD),(D^cu^c)$: Leptoquark and diquark. Box diagram can contribute to flavor-changing processes and nucleon decay.

(ii) $\tilde{e}^-(1,3,-2)$: $(e^+L_1^0),(uD^c),(N^cL_2^+)$: Mixes SM and exotic leptons and quarks. Exchange can contribute to $e^+e^- \to L_1^{0c}L_2^0$

(iii) $\tilde{u}(1,-1,-1)$: $(d^cL_1^-),(e^-D^c),(dD),(u^cL_2^{0c})$: Leptoquark and diquark. Box diagram contributing to nucleon decay with $dd \to L_1^-D^c$ ($\tilde{u}$ exchange) followed by $L_1^-h_c \to u^c\nu_c$ ($\tilde{d}$ exchange)

(iv) $\tilde{d}(1,-1,-1)$: $(d^cL_1^0),(\nu D^c),(uD),(u^cL_2^+)$: Leptoquark and diquark. Box diagram contributing to nucleon decay with $uu \to L_2^+D^c$ ($\tilde{d}$ exchange) followed by $L_2^+D^c \to d^ce^+$ ($\tilde{u}$ exchange)

(v) $\tilde{u}^c(1,-1,-1)$: $(d^cD^c),(e^+D),(dL_2^+),(uL_2^{0c})$: Leptoquark and diquark. Box diagram contributing to nucleon decay.

(vi) $\tilde{e}^+(1,-1,-1)$: $(e^-L_1^0),(\nu L^-),(Du^c)$: Mixes SM and exotic leptons and quarks. Exchange can contribute to $e^+e^- \to L_1^0L_2^{0c}$.

(vii) $\tilde{D}^c(-2,-2,3)$: $(d^cu^c),(e^-u),(\nu d),(nD)$: Leptoquark and diquark; induces proton decay.

(viii) $\tilde{L}_1^-(-2,-2,3)$: $(d^cu),(\nu e^+),(L_2^+n)$: Charged Higgs boson.

(ix) $\tilde{D}(-2,2,2)$: $(d^cN^c),(e^+u^c),(du),(D^cn)$: Leptoquark and diquark; induces proton decay.

(x) $\tilde{L}_2^+(-2,2,2)$: $(e^-N^c),(du^c),(L_1^-n)$: Charged Higgs boson.

Many of the scalars, when exchanged, can contribute to the pair production of exotic fermions [those in the 10 or 1 of SO(10)]. However, if these exotic fermions have masses of order TeV or greater, they can have escaped detection up to now. In subsequent sections we discuss the theoretical and experimental constraints on the Yukawa couplings and masses of these fermions. Theoretical constraints of perturbativity at unification scale set the upper bound on these masses, while the experimental searches for vectorlike quarks, long-lived charged particles, and squarks lead to lower bounds on the masses.

More dangerous are the scalars $\tilde{D}$ and $\tilde{D}^c$, whose exchange can lead, for example, to the subprocess $du \to \bar{u}e^+$ and thus to $p \to e^+\pi^0$. The simplest way to deal with this problem is to assume those scalars have masses at the GUT scale. This prevents them from being supersymmetric partners of the vectorlike quarks D and D^c; in other words our model does not possess TeV-scale supersymmetry. One then has to prevent the Higgs bosons [belonging to the same SU(5) 5- or $\bar{5}$-plet as $\tilde{D}$ or $\tilde{D}^c$] from acquiring large masses as well. We shall not confront this hierarchy problem here but an eventual solution is necessary.

IV. SCALAR POTENTIAL AND BOSON MASSES

As described above, the low-energy mass spectrum of the E_6 model consists of neutral scalars and charged and neutral fermions, so signatures for the neutral scalar SO(10) singlet $\tilde{n}$ are an important feature of the model. Such a scalar is constrained by its mixing with the SM Higgs particle in the gluon fusion channel. In this section we investigate such a constraint as well as the nature of such a scalar: whether it is a real scalar or pseudoscalar in the light of a possible future discovery at or below the TeV scale. A Z_N gauge boson is another important TeV-scale prediction of the model, so its mass and its relation with the $\tilde{n}$ scalars are discussed as well.

A. Scalar potential

The field $\tilde{n}$ is complex and may be resolved into scalar and pseudoscalar components. A scalar can mix with the SM Higgs boson, in which case its $\gamma\gamma$ branching fraction becomes diluted by other decay modes such as $t\bar{t}$ and tree-level decays to the SM vector bosons. This is accompanied by the reduction of the tree-level SM Higgs couplings to these particles. This results in constraints on the couplings of this new resonance due to measurements of Higgs boson couplings at the LHC as well as LHC searches for a new heavy Higgs boson decaying to a pair of SM bosons. One estimate [123] finds the allowed mixing angle to be less than 0.1. This problem is avoided if the $\tilde{n}$ state is taken to be a pseudoscalar, which requires addition of another singlet or finding an alignment limit to turn off the mixing in the scalar sector itself. We shall explore both possibilities.

The five complex scalar fields $\phi = (\tilde{\nu}\ \tilde{N}^c\ \tilde{L}_1^0\ \tilde{L}_2^c\ \tilde{n})$ neutral under the SM symmetry of $SU(3)_c \otimes U(1)_{\rm em}$ are summarized for convenience in Table III. A scalar potential can be written in terms of these fields and their conjugates ϕ^c. The most general renormalizable scalar potential that obeys E_6 symmetry at the unification scale breaking down to $SU(3)_c \otimes SU(2)_L \otimes U(1)_{\rm em} \otimes U(1)_N$ at the TeV scale can be written as

$$\begin{aligned} V = {} & \frac{m_1^2}{2}\tilde{\nu}\tilde{\nu}^c + \frac{m_2^2}{2}\tilde{N}^c\,\tilde{N} + \frac{m_3^2}{2}\tilde{L}_1^0\tilde{L}_1^{0c} + \frac{m_4^2}{2}\tilde{L}_2^0\tilde{L}_2^{0c} + \frac{m_5^2}{2}\tilde{n}\tilde{n}^c + a_1\tilde{N}^c\,\tilde{\nu}\,\tilde{L}_2^0 + a_2\tilde{N}\tilde{\nu}^c\tilde{L}_2^{0c} + a_3\tilde{L}_1^0\,\tilde{L}_2^0\,\tilde{n} + a_4\tilde{L}_1^{0c}\tilde{L}_2^{0c}\tilde{n}^c \\ & + \frac{b_1}{2}\tilde{N}^c\,\tilde{\nu}\,\tilde{L}_1^{0c}\tilde{n}^c + \frac{b_2}{2}\tilde{N}\tilde{\nu}^c\tilde{L}_1^0\,\tilde{n} + \frac{b_3}{2}\tilde{L}_1^0\tilde{L}_1^{0c}\tilde{n}\tilde{n}^c + \frac{b_4}{2}\tilde{L}_2^0\tilde{L}_2^{0c}\tilde{n}\tilde{n}^c + \frac{b_5}{2}\tilde{\nu}\tilde{\nu}^c\tilde{n}\tilde{n}^c + \frac{b_6}{2}\tilde{N}^c\,\tilde{N}\,\tilde{n}\,\tilde{n}^c + \frac{b_7}{4}\tilde{\nu}\,\tilde{\nu}\,\tilde{\nu}^c\tilde{\nu}^c \\ & + \frac{b_8}{2}\tilde{\nu}\,\tilde{N}^c\,\tilde{\nu}^c\tilde{N} + \frac{b_9}{4}\tilde{N}^c\,\tilde{N}^c\,\tilde{N}\,\tilde{N} + \frac{b_{10}}{2}\tilde{\nu}\tilde{\nu}^c\tilde{L}_1^0\tilde{L}_1^{0c} + \frac{b_{11}}{2}\tilde{\nu}\tilde{\nu}^c\tilde{L}_2^0\tilde{L}_2^{0c} + \frac{b_{12}}{2}\tilde{N}^c\,\tilde{N}\,\tilde{L}_1^0\,\tilde{L}_1^{0c} + \frac{b_{13}}{2}\tilde{N}^c\,\tilde{N}\,\tilde{L}_2^0\,\tilde{L}_2^{0c} \\ & + \frac{b_{14}}{2}\tilde{L}_1^0\tilde{L}_1^{0c}\tilde{L}_2^0\tilde{L}_2^{0c} + \frac{b_{15}}{4}\tilde{L}_1^0\tilde{L}_1^{0c}\tilde{L}_1^0\tilde{L}_1^{0c} + \frac{b_{16}}{4}\tilde{L}_2^0\tilde{L}_2^{0c}\tilde{L}_2^0\tilde{L}_2^{0c} + \frac{b_{17}}{4}\tilde{n}\,\tilde{n}\,\tilde{n}^c\tilde{n}^c. \end{aligned} \tag{7}$$

Quadratic terms come from the product $27 \otimes \overline{27}$; trilinear terms come from the product $27 \otimes 27 \otimes 27$ or its charge conjugate; quartic terms come from $27 \otimes 27 \otimes \overline{27} \otimes \overline{27}$. Fifteen of the 17 quartic terms are of the form $(\phi_a^c\phi_a)(\phi_b^c\phi_b)$. The remaining two terms, with coefficients b_1 and b_2, are the only additional ones found invariant when E_6 breaks down to SO(10) and SU(5).

At the weak scale $SU(2)_L$ and $U(1)_N$ are broken spontaneously. The spontaneous symmetry breaking of all the fields will generate the corresponding mass matrix $\mathcal{M}$:

$$V = \frac{1}{2}s_i\mathcal{M}s_j, \quad \text{where } \mathcal{M} = 2\frac{\partial^2 V}{\partial s_i \partial s_j} \quad \text{and} \quad s = (\phi_i, \phi_i^c). \tag{8}$$

We convert this basis to that of ten real fields corresponding to real (scalar) and imaginary (pseudoscalar) parts of the five complex fields ϕ_i, as follows:

$$\mathcal{M}_{rf} = R^T\mathcal{M}R, \quad \text{where } R = \frac{1}{\sqrt{2}}\begin{pmatrix} \mathbb{I}_{5\times5} & i\mathbb{I}_{5\times5} \\ \mathbb{I}_{5\times5} & -i\mathbb{I}_{5\times5} \end{pmatrix}. \tag{9}$$

As described in Sec. II B, $\mathbb{Z}_2$ symmetry leads to $\langle\tilde{\nu}\rangle$, $\langle\tilde{N}\rangle = 0$. In addition, we assume the potential is CP even. This translates into $a_1 = a_2 \equiv a'$, $a_3 = a_4 \equiv a$, and $b_1 = b_2 \equiv b$. These conditions result in the separation of the scalars in the 16 representation of SO(10) from the other three. The elements of the corresponding 2×2 and 3×3 mass matrices for the real parts are

$$\begin{aligned} \mathcal{M}^s_{\tilde{\nu}\tilde{\nu}} &= m_1^2 + b_5\langle\tilde{n}\rangle^2 + b_{10}v_d^2 + b_{11}v_u^2, \\ \mathcal{M}^s_{\tilde{\nu}\tilde{N}} &= \mathcal{M}^s_{\tilde{N}\tilde{\nu}} = 2a'v_u + bv_d\langle\tilde{n}\rangle, \\ \mathcal{M}_{\tilde{N}\tilde{N}} &= m_2^2 + b_6\langle\tilde{n}\rangle^2 + b_{12}v_d^2 + b_{13}v_u^2; \end{aligned} \tag{10}$$

$$\begin{aligned} \mathcal{M}^s_{\tilde{L}_1\tilde{L}_1} &= m_3^2 + b_3\langle\tilde{n}\rangle^2 + b_{14}v_u^2 + 3b_{15}v_d^2, \\ \mathcal{M}^s_{\tilde{L}_1\tilde{L}_2} &= \mathcal{M}^s_{\tilde{L}_2\tilde{L}_1} = 2(a\langle\tilde{n}\rangle + b_{14}v_dv_u), \\ \mathcal{M}^s_{\tilde{L}_2\tilde{L}_2} &= m_4^2 + b_4\langle\tilde{n}\rangle^2 + b_{14}v_d^2 + 3b_{16}v_u^2, \\ \mathcal{M}^s_{\tilde{L}_1\tilde{n}} &= \mathcal{M}^s_{\tilde{n}\tilde{L}_1} = 2(av_u + b_3v_d\langle\tilde{n}\rangle), \\ \mathcal{M}^s_{\tilde{L}_2\tilde{n}} &= \mathcal{M}^s_{\tilde{n}\tilde{L}_2} = 2(av_d + b_4v_u\langle\tilde{n}\rangle), \\ \mathcal{M}^s_{\tilde{n}\tilde{n}} &= m_5^2 + b_3v_d^2 + b_4v_u^2 + 3b_{17}\langle\tilde{n}\rangle^2. \end{aligned} \tag{11}$$

The mass matrices for the pseudoscalar parts are

$$\begin{aligned} \mathcal{M}^p_{\tilde{\nu}\tilde{\nu}} &= m_1^2 + b_5\langle\tilde{n}\rangle^2 + b_{10}v_d^2 + b_{11}v_u^2, \\ \mathcal{M}^p_{\tilde{\nu}\tilde{N}} &= \mathcal{M}^p_{\tilde{N}\tilde{\nu}} = -2a'v_u - bv_d\langle\tilde{n}\rangle, \\ \mathcal{M}^p_{\tilde{N}\tilde{N}} &= m_2^2 + b_6\langle\tilde{n}\rangle^2 + b_{12}v_d^2 + b_{13}v_u^2; \end{aligned} \tag{12}$$

$$\begin{aligned} \mathcal{M}^p_{\tilde{L}_1\tilde{L}_1} &= m_3^2 + b_3\langle\tilde{n}\rangle^2 + b_{14}v_u^2 + b_{15}v_d^2, \\ \mathcal{M}^p_{\tilde{L}_1\tilde{L}_2} &= \mathcal{M}^p_{\tilde{L}_2\tilde{L}_1} = -2a\langle\tilde{n}\rangle, \\ \mathcal{M}^p_{\tilde{L}_2\tilde{L}_2} &= m_4^2 + b_4\langle\tilde{n}\rangle^2 + b_{14}v_d^2 + b_{16}v_u^2, \\ \mathcal{M}^p_{\tilde{L}_1\tilde{n}} &= \mathcal{M}^p_{\tilde{n}\tilde{L}_1} = -2av_u, \\ \mathcal{M}^p_{\tilde{L}_2\tilde{n}} &= \mathcal{M}^p_{\tilde{n}\tilde{L}_2} = -2av_d, \\ \mathcal{M}^p_{\tilde{n}\tilde{n}} &= m_5^2 + b_3v_d^2 + b_4v_u^2 + b_{17}\langle\tilde{n}\rangle^2, \end{aligned} \tag{13}$$

where $v^2 = v_u^2 + v_d^2$ and $v = 246$ GeV.

TABLE III. Neutral complex scalar fields belonging to the 27-plet or $\overline{27}$-plet of E_6.

	27 member			$\overline{27}$ member		
State	$2\sqrt{10}Q_N$	I_{3L}	State	$2\sqrt{10}Q_N$	I_{3L}	$\mathbb{Z}_2$
$\tilde{\nu}$	-2	$1/2$	$\tilde{\nu}^c$	2	$-1/2$	-1
$\tilde{N}^c$	0	0	$\tilde{N}$	0	0	-1
$\tilde{L}_1^0$	3	$1/2$	$\tilde{L}_1^{0c}$	-3	$-1/2$	1
$\tilde{L}_2^{0c}$	2	$-1/2$	$\tilde{L}_2^0$	-2	$1/2$	1
$\tilde{n}$	-5	0	$\tilde{n}^c$	5	0	1

The SM Higgs boson is a part of the doublet of the real scalars. Thus, in order to avoid the constraints due to SM Higgs production and decays, we would like to turn off the mixing between the two Higgs doublets and the SO(10) singlet. From Eq. (11) we see that this requires

$$\tan^2\beta = \frac{b_3}{b_4}, \quad \text{where } \tan\beta = \frac{v_u}{v_d}. \tag{14}$$

This also needs b_3 and b_4 to have a sign opposite to that of a. On the other hand, the pseudoscalar sector mixings disappear when $a = 0$. Thus the only way to avoid doublet-singlet mixing in both real scalar and pseudoscalar sectors is the *ad hoc* imposition of $a = b_3 = b_4 = 0$.

We will not discuss this case further as it completely decouples $\tilde{n}$ from the SM Higgs boson and, thus, is not very interesting from the point of view of LHC discovery. In the following we explore constraints on the Lagrangian parameters in the other scenarios with small mixing. Such an analysis will also be important in the context of supersymmetric E_6 models [46], where the parameter definitions are constrained by the gauge coupling constants.

We note that for $a = 0$ the pseudoscalar mixings are turned off. This implies that the Goldstone boson associated with the breaking of the $U(1)_N$ symmetry will have to be the singlet pseudoscalar. It forces us to identify $\tilde{n}$ with the real singlet scalar that mixes with the SM Higgs. The fits to the LHC Higgs coupling measurements and the heavy Higgs searches in the WW and ZZ channel [123,124] impose an upper bound on the parameters b_3 and b_4 for a given mass spectrum. These are relaxed in the decoupling limit, where the mass of the CP-odd Higgs (M_A) is taken to several TeV.

Another possibility is to add an additional singlet complex scalar field with the same quantum numbers as that of $\tilde{n}$. This extra singlet can be part of an additional scalar 27-plet that can be added to the model. Assigning a TeV-scale vacuum value to such a singlet will decouple it from the SM Higgs. The imaginary component of this singlet can serve as the required Goldstone boson corresponding to the spontaneous breaking of the $U(1)_N$ symmetry, thus making the pseudoscalar corresponding to the original singlet available at sub-TeV masses which can be discovered at the LHC. The real scalar corresponding to this pseudoscalar singlet can now be made much heavier than 1 TeV, even if a sub-TeV scalar resonance is found, thus leading to its decoupling from the SM Higgs boson and relaxation of the constraints on b_3 and b_4.

A third possibility is to turn the mixing in the scalar sector off by imposing

$$\tan^2\beta = \frac{b_3}{b_4} \quad \text{and} \quad a = -\frac{b_3\langle\tilde{n}\rangle}{\tan\beta}. \tag{15}$$

In the event of a sub-TeV scalar discovery, this case still allows for the required pseudoscalar Goldstone boson associated with the $U(1)_N$ breaking without the addition of an extra singlet. Additional constraints on b_3 and b_4 will originate from the constraints on $\tan\beta$ and that on a due to the fact that the global minimum (or local up to metastability) of the complete scalar potential needs to be that corresponding to the SM electroweak symmetry-breaking minimum.

B. Gauge boson masses

The covariant derivative for this model is given by

$$D_\mu = \partial_\mu - ig\tau^a W_\mu^a - ig' Y B_\mu - ig_N Y_N B'_\mu. \tag{16}$$

The scalar kinetic term in the Lagrangian that leads to the gauge boson mass matrix is

$$\mathcal{L} \supset (D^\mu \tilde{L_1})^\dagger (D_\mu \tilde{L_1}) + (D^\mu \tilde{L_2})^\dagger (D_\mu \tilde{L_2}) + (D^\mu \tilde{n})^\dagger (D_\mu \tilde{n}). \tag{17}$$

The charged gauge boson sector in this model remains identical to the standard model. The neutral boson sector has an additional massive Z_N boson due to spontaneous breaking of the $U(1)_N$ symmetry. The mass matrix is as follows:

$$\mathcal{M} = \begin{pmatrix} (g^2v^2)/4 & (gg'v^2)/4 & [gg_N(y_{N_1}v_d^2 + y_{N_2}v_u^2)]/2 \\ (gg'v^2)/4 & (g'^2v^2)/4 & [g'g_N(y_{N_1}v_d^2 + y_{N_2}v_u^2)]/2 \\ \frac{gg_N(y_{N_1}v_d^2+y_{N_2}v_u^2)}{2} & \frac{g'g_N(y_{N_1}v_d^2+y_{N_2}v_u^2)}{2} & (g_N)^2(y_{N_1}^2v_d^2 + y_{N_2}^2v_u^2 + y_{N_s}^2\langle\tilde{n}\rangle^2) \end{pmatrix}, \tag{18}$$

where y_{N_1}, y_{N_2} and y_{N_s} are Q_N charges for the exotic lepton doublets and SO(10) singlet, respectively.

Current lower bounds on $M(Z_N)$ are ~2.5 TeV based on 7 and 8 TeV data [107,108], and about 1 TeV higher based on 13 TeV data up to mid-July 2016 [109,110]. [A lower bound on $M(Z_N)$ quoted at the March 2017 Moriond Electroweak meeting, based on about 1/3 of the 13 TeV sample, was 3.41 TeV [111]; a recent ATLAS lower bound based on 36.1 fb^{-1} is 3.8 TeV [112].] As noted in [46] the natural value of g_N is less than one. Another issue is the mixing of the new Z_N boson with the SM neutral gauge bosons. We need the photon to be massless; the mass of the

Z boson is measured with ∼0.001% precision. Thus the mixing needs to be small enough in order to obey these bounds. This implies that g_N needs to be much smaller than one.

To satisfy the experimental lower bound on $M(Z_N)$, we can either have $\langle\tilde{n}\rangle$ of order several TeV, which in turn will impose lower bounds upon the mass of the singlet scalar due to requirement of the vacuum stability as explained in Sec. V, or we can add another singlet charged under $U(1)_N$. This can be the SO(10) singlet of the 351′-plet of scalars. Let us denote it by S. As described in the previous section, such an addition also helps with identifying the LHC-detectable $\tilde{n}$ candidate as a pseudoscalar without going to the alignment limit in the scalar sector or *ad hoc* imposing $a = b_3 = b_4 = 0$.

Such a singlet will add a term $(g_N)^2 y_{N_s}^2 \langle S\rangle^2$ to the diagonal element corresponding to the Z_N mass. The gauge coupling evolution shown in Fig. 10 [Appendix C] gives the value of α_N^{-1} at the experimental lower bound of the Z_N boson mass to be ∼86. This means

$$g_N^2 = \frac{4\pi}{86} \approx 0.146 \tag{19}$$

at that lower bound. This singlet has a Q_N charge of $10/\sqrt{40}$. Thus, a lower bound on the Z_N mass of ∼4 TeV [107–112] (details in Sec. X) puts a lower bound on the VEV of such a singlet:

$$\langle S\rangle > \sqrt{\frac{16}{(0.146)(100/40)}} \sim 6.6 \text{ TeV}. \tag{20}$$

This new vacuum value will decouple the Z_N from the SM neutral gauge bosons, solving both the problem of mixing with the Z boson and the lower mass bound on Z_N.

V. RENORMALIZATION GROUP EVOLUTION

It is necessary to calculate the renormalization group evolution (RGE) of both the gauge couplings and the Yukawa couplings to ensure that they remain perturbative at electroweak energy scales and all the way up to the unification scale (10^{16} GeV) or the Planck scale (10^{19} GeV). Thus, the lowest energy scales at which the Landau poles are permitted to occur can be taken as these scales to obtain corresponding electroweak-scale upper bounds on the values of the Yukawa couplings for the exotic fermions.

The beta functions of the quartic couplings of the type b_i in the scalar potential enumerated in Sec. IV receive negative contributions from the exotic Yukawa couplings. This can lead to the quartic couplings running to negative values at energy scales much lower than the unification scale, making the vacuum unstable at these lower scales. Some new physics beyond the E_6 framework would be necessary to restore the vacuum stability. In order to avoid this and preserve the E_6 features up to the unification scale, the quartic couplings will have lower bounds at the electroweak (EW) scale such that they do not turn negative at energies below the unification scale. The RGE of the quartics is necessary to compute these lower bounds. These quartics also have an upper bound due to the presence of the b_i^2 terms with positive coefficients in the beta function which can lead to poles below the unification scales. The details of these calculations for exotic Yukawa and quartic couplings are given in Appendix C. We present the main results here.

We find that it is hard to push the upper bound of the vectorlike quark mass above 750 GeV, if we demand perturbative Yukawa coupling constants at least up to 10^{16} GeV. The lower bounds on the vectorlike quark masses set by CMS and ATLAS at the LHC are close to, but higher than, 750 GeV and depend on the branching ratio to W + SM and H + SM [125,126]. Thus, in order for this model to be a viable theory up to the GUT scale, it is necessary to avoid these bounds.

This is achieved if the vectorlike particles are protected by a $\mathbb{Z}_2$ symmetry, which forbids vertices such as DqW, DqZ and DqH. This can lead to another problem. In the absence of these decays, the exotic quarks are subject to the cross section bounds on long-lived charged particles. As discussed in Sec. IX A, these bounds are even higher than those placed by the vectorlike quark searches. This problem is circumvented by $\mathbb{Z}_2$-preserving decays as follows.

As explained in Sec. IX A, $\mathbb{Z}_2$-preserving decays of the exotic quarks to the SM quarks and $\tilde{\nu}$ or $\tilde{N}^c$ allow one to escape the long-lived charged particle bounds. They open up a window of viable exotic quark masses with a lower bound of ∼400 GeV as discussed in Sec. IX A. Demanding the unification-scale perturbativity of the Yukawa couplings implies an upper bound of 1.3 on the exotic Yukawa couplings at the electroweak scale. As the exotic fermion masses are given by $y_i\langle\tilde{n}\rangle$, this sets the upper bound of this window proportional to $\langle\tilde{n}\rangle$. This upper bound on mass is constrained by the vacuum stability considerations for a given mass of $\tilde{n}$ as follows.

From Eq. (B5), for small b_3, b_4 and a single scalar generation, we have

$$b_{17} = \frac{m_{\tilde{n}}^2}{2\langle\tilde{n}\rangle^2}. \tag{21}$$

For a lower bound of b_{17} for b_{17} at the EW scale, we have an upper bound on the allowed $\langle\tilde{n}\rangle$ for a given mass of $\tilde{n}$. Its value is

$$\langle\tilde{n}\rangle = \frac{m_{\tilde{n}}}{\sqrt{2b_{17}}}. \tag{22}$$

Thus, the exclusion due to the vacuum stability constraint is characterized by a straight line of slope $1/\sqrt{2b_{17}}$ passing through the origin on the $\langle\tilde{n}\rangle - m_{\tilde{n}}$ plot with the area above the line excluded. The slope of the line decreases with

increasing EW-scale values of the exotic Yukawa couplings as a larger and larger region is excluded. From the example in Appendix C we see that for the exotic Yukawa coupling of 0.95 for quarks and 0.95 for the leptons we get the lower bound of 1.4 on b_{17}, which leads to an upper bound of $\sim 0.63 m_{\tilde{n}}$ on the SO(10) scalar singlet ($\tilde{n}$) VEV. More details of bounds related to b_{17} and its connection to bounds on Yukawa couplings and therefore the mass spectrum are discussed in Sec. XI.

In this window of 400 GeV to $1.3\langle\tilde{n}\rangle$, the mass of the SO(10) 16-plet neutral scalar $\tilde{\nu}$ or $\tilde{N}^c$ is constrained to be almost degenerate with the vectorlike quark mass for masses lower than 500 GeV. This result is obtained by recasting the LHC searches as discussed in Sec. IX. Thus, the mass of the SO(10)-singlet scalar constrains the rest of the spectrum via vacuum stability considerations.

Finally, the standard-model Higgs coupling is unaffected by the addition of the new particles, as the additional fermions do not have tree-level Yukawa couplings to the doublet Higgs boson. Thus the danger of the doublet Higgs quartic coupling going to negative values at the TeV scale is avoided. The mixing of the Higgs doublet with the singlet may lead to positive contributions to the doublet quartic beta functions. As discussed in Sec. IV, this mixing is constrained to be a small value by the experimental bounds and will not pose a problem for the stability of the doublet Higgs quartic coupling.

VI. DECAYS OF $\tilde{n}$ TO $\gamma\gamma$, γZ, ZZ, W^+W^-, ZH

The coupling of $\tilde{n}$ to a loop of the exotic lepton L generates decays to other pairs of electroweak gauge bosons besides $\gamma\gamma$, namely $Z\gamma$, ZZ, and WW. For general discussions of the ratio of the corresponding partial widths see [80,82,127–129]. The gauge-invariant terms in the Lagrangian describing the most general couplings of $\tilde{n}$ to electroweak bosons W and B may be written

$$\delta\mathcal{L}_{\rm ew} = \frac{\alpha_{\rm em}}{4\pi x}\frac{\kappa_W}{4m_{\tilde{n}}}\tilde{n}W^a_{\mu\nu}W^{a\mu\nu} + \frac{\alpha_{\rm em}}{4\pi(1-x)}\frac{\kappa_B}{4m_{\tilde{n}}}\tilde{n}B_{\mu\nu}B^{\mu\nu},$$
$$x \equiv \sin^2\theta_W. \tag{23}$$

With $Z = W^3\cos\theta_W - B\sin\theta_W$, $A = W^3\sin\theta_W + B\cos\theta_W$, the couplings are

$$g_{\tilde{n}\gamma\gamma} = C_0(\kappa_W + \kappa_B), \tag{24}$$

$$g_{\tilde{n}Z\gamma} = C_0\sqrt{x(1-x)}\left(\frac{\kappa_W}{x} - \frac{\kappa_B}{1-x}\right), \tag{25}$$

$$g_{\tilde{n}ZZ} = C_0\left(\kappa_W\frac{1-x}{x} + \kappa_B\frac{x}{1-x}\right), \tag{26}$$

$$g_{\tilde{n}WW} = C_0\left(\frac{\kappa_W}{x}\right), \tag{27}$$

TABLE IV. Vector and axial-vector couplings of fermions for L^+L^- and $L^0\bar{L}^0$ production.

	Fermion					
	u quark		d quark		L^- lepton	L^0 lepton
Boson	C_V	C_A	C_V	C_A	C_V	C_V
γ	$2e/3$	0	$-e/3$	0	$-e$	0
Z^0	$g_Z(\frac{1}{4}-2x/3)$	$-g_Z/4$	$g_Z(-\frac{1}{4}+x/3)$	$g_Z/4$	$g_Z(-\frac{1}{2}+x)$	$g_Z/2$

where C_0 is a common factor. Taking account of the contribution of three charged vectorlike L states in the loop, the ratio of $Z\gamma$ and $\gamma\gamma$ couplings is found (cf. Table IV) to be

$$\frac{g_{\tilde{n}Z\gamma}}{g_{\tilde{n}\gamma\gamma}} = [x(1-x)]^{-1/2}\left(\frac{1}{2}-x\right), \tag{28}$$

consistent with $\kappa_B = \kappa_W$. Adding the contribution of three $Q = -1/3$ weak isoscalar quarks ("$D_{1,2,3}$"), one finds instead $\kappa_B = (5/3)\kappa_W$. In this case, substituting $x = 0.2315$, squaring amplitudes, and multiplying by 2 for nonidentical particles in the final state, one finds partial decay rates to be in the ratio

$$\Gamma_{\gamma\gamma}:\Gamma_{Z\gamma}:\Gamma_{ZZ}:\Gamma_{WW} = 1:0.24:2.08:5.32. \tag{29}$$

Similar results (aside from a factor of 2 lower for $Z\gamma$) were obtained in Ref. [130]. These ratios should be targets for discovery or bounds when the LHC accumulates more data at 13 TeV. As shown in Fig. 2 and explained in Sec. VII, $\sigma(pp \to \tilde{n} \to \gamma\gamma)$ is excluded for values greater than 1 fb due to ATLAS (15.6 fb^{-1} at 13 TeV) [39] and CMS (16.2 fb^{-1} at 13 TeV + 19.7 fb^{-1} at 8 TeV) [41] searches and vacuum stability constraints. In the present context of probing for the EW- and TeV-scale signatures of the E_6 model at the LHC, we see that the present upper bound on $\sigma(pp \to \tilde{n}X)\mathcal{B}(\tilde{n} \to W^+W^-)$ [131] is greater than 10 fb, corresponding to a $WW/\gamma\gamma$ ratio of at least 10. For $\sigma(pp \to \tilde{n}X \to Z\gamma X)$, an upper limit for a narrow $\tilde{n}$ is at least about 20 fb [132], a factor of $\sim$100 above expectation based on Eq. (29) and the fact that the $\gamma\gamma$ cross section is less than 1 fb. Therefore, these channels are much less sensitive to the discovery of $\tilde{n}$ if it exists at TeV or sub-TeV scales, thus making $\gamma\gamma$ the most significant channel for discovery.

An interesting point has been raised in Ref. [133]. It was found there that a spinless particle S which is a SM singlet can decay to Z + (Higgs boson) only if it has CP-odd interactions. If so, the $S \to ZH$ rate could even surpass that for $S \to \gamma\gamma$.

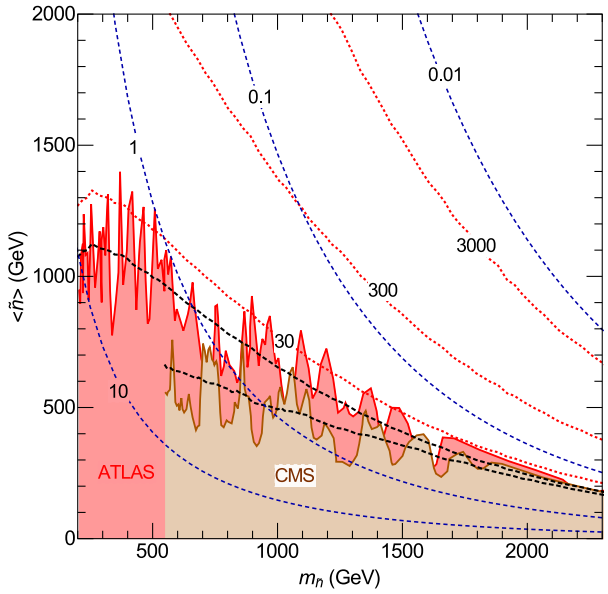

FIG. 2. Dark [red] and lighter [dark orange] shaded regions show the exclusion regions for exotics by ATLAS [39,40] and CMS [41], respectively, in the diphoton channel. Black (dashed) curve: Expected 95% exclusion limit for ATLAS (upper curve, 15.6 fb^{-1} at 13 TeV) and CMS (lower curve, 16.2 fb^{-1} at 13 TeV + 19.7 fb^{-1} at 8 TeV). Red (dotted) curve: Contours showing ATLAS reach for nondiscovery for luminosities of 30, 300 and 3000 fb^{-1} at 13 TeV. Blue (dashed) curve: Contours of constant cross section $\sigma_0 \equiv \sigma(pp \to \tilde{n}X \to \gamma\gamma X)$ in the plane of $\langle\tilde{n}\rangle$ versus $m_{\tilde{n}}$ for values of σ_0, top to bottom, ranging from 0.01 to 10 fb.

VII. PRODUCTION OF $\tilde{n}$ AND $\gamma\gamma$ DECAY

We discuss the production of the scalar member $\tilde{n}$ of an E_6 27-plet, transforming as an SU(5) and SO(10) singlet. Among its decay channels, we focus on the $\gamma\gamma$ mode as it is the most sensitive to the discovery of such a singlet among all the decay modes as described in the previous section. If Q_N is respected in its couplings, it does not couple to pairs of ordinary fermions in the 16-plet of SO(10), but only to the exotic fermions D and L. (In supersymmetric E_6 versions, the L states may be identified as Higgsinos, while the $\tilde{L}$ are the two Higgs doublets [46].) Then $\tilde{n}$ can be produced via gluon-gluon fusion via loops containing D quarks, one for each of the three families. It can decay to two photons via D quarks and exotic leptons $L^{\pm}$ in loops, as shown in Fig. 3. We then need expressions for

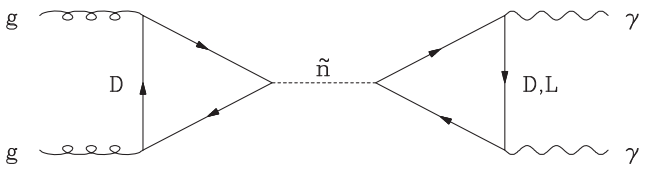

FIG. 3. Mechanism for hadronic production and decay of scalar boson $\tilde{n}$.

$\Gamma(\tilde{n} \to gg)$, $\Gamma(\tilde{n} \to \gamma\gamma)$, and the effective two-gluon luminosity in proton-proton collisions. We shall rely on the treatment in Ref. [134]. (For a discussion of an alternative mechanism for $\tilde{n}$ production via the $\gamma\gamma$ initial state see, e.g., Refs. [135–140].)

Two of the neutral companions of the scalar $\tilde{n}$ in the 27-plet are the Higgs bosons in a conventional two-Higgs-doublet model. We assume each D_i, where $i = 1$, 2, 3 is the family label, is coupled to $\tilde{n}$ via a term $\Delta\mathcal{L} = y_{D_i}\tilde{n}\bar{D}_i D_i$. One then finds

$$\Gamma(\tilde{n} \to gg) = \left(\frac{\alpha_s}{6\pi}\right)^2 \frac{m_{\tilde{n}}^3}{2\pi}\left(\sum_{i=1}^{3}\frac{y_{D_i}}{m_{D_i}}F_+(\beta_i)\right)^2, \quad (30)$$

where $\beta_i \equiv (2m_{D_i}/m_{\tilde{n}})^2$, and for a scalar $\tilde{n}$ [141,142],

$$F_+(\beta) \equiv \frac{3}{2}\beta\left[1 + (1-\beta)\arcsin^2\frac{1}{\sqrt{\beta}}\right]. \quad (31)$$

For a pseudoscalar $\tilde{n}$ (see, e.g., [143,144]),

$$F_-(\beta) = \beta\arcsin^2(1/\sqrt{\beta}). \quad (32)$$

These functions are plotted in the left panel of Fig. 4. Both $F_+(\beta)$ and $F_-(\beta)$ approach 1 for large β. We do not consider the case $\beta < 1$, in which $\tilde{n} \to D\bar{D}$ becomes kinematically allowed.

We now assume that each D_i obtains its mass through the VEV $\langle\tilde{n}\rangle$ of $\tilde{n}$ itself. This is the only neutral 27-plet member whose VEV can give mass to the exotic fermions D and L, as noted at the end of Sec. II. In this case one has $y_{D_i}/m_{D_i} = 1/\langle\tilde{n}\rangle$, and the expression for $\Gamma(\tilde{n} \to gg)$ reduces to

$$\Gamma(\tilde{n} \to gg) = \left(\frac{\alpha_s}{6\pi}\right)^2 \frac{m_{\tilde{n}}^3}{2\pi\langle\tilde{n}\rangle^2}\left(\sum_{i=1}^{3}F_{\pm}(\beta_i)\right)^2. \quad (33)$$

While QCD corrections to this partial width are appreciable—about a factor of 2 [134]—they will largely cancel out when we express the cross section for $pp \to \tilde{n}X \to \gamma\gamma X$ in terms of the partial width $\Gamma(\tilde{n} \to \gamma\gamma)$.

We next evaluate the cross section for $\tilde{n}$ production in pp collisions at the LHC. Reference [134] defines a gluon-gluon luminosity as an integral over the rapidity y at which $\tilde{n}$ is produced:

$$\left.\frac{dL_{gg}}{d\hat{s}}\right|_{\hat{s}=m_{\tilde{n}}^2} \equiv \frac{1}{s}\int_{\ln\sqrt{\tau}}^{\ln 1/\sqrt{\tau}} dy g(x_1, Q^2)g(x_2, Q^2), \quad (34)$$

where $x_1 \equiv \sqrt{\tau}e^y$, $x_2 = \tau/x_1$, $\tau \equiv m_{\tilde{n}}^2/s$, and s is the square of the total c.m. energy. Here $g(x, Q^2)$ is the gluon structure

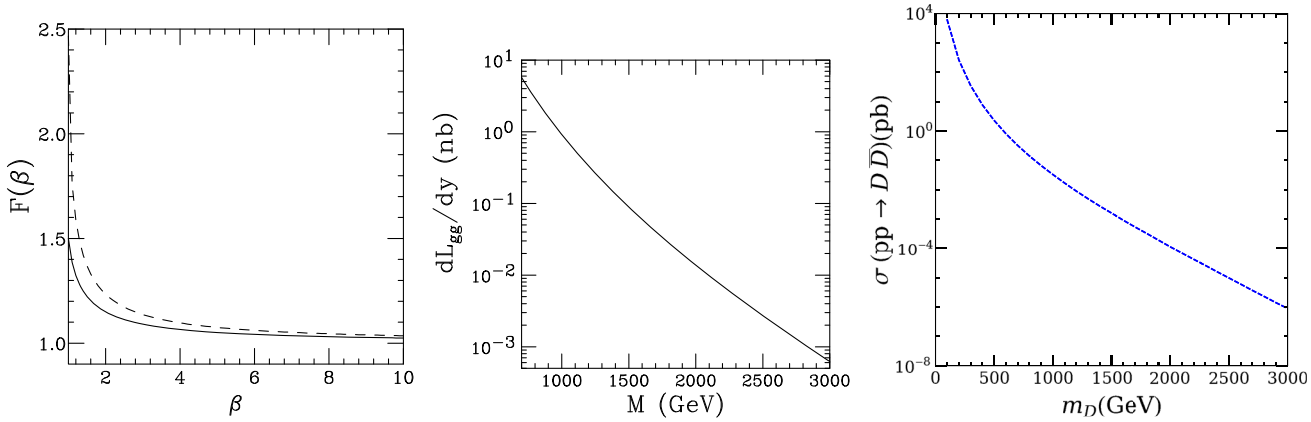

FIG. 4. Left: Functions $F_{\pm}(\beta)$ governing decays of scalar (F_+) or pseudoscalar (F_-) to two photons. Solid curve, scalar $\tilde{n}$; dashed curve, pseudoscalar $\tilde{n}$. Middle: Effective gluon-gluon luminosity function for proton-proton production of a state with mass M at center-of-mass energy $\sqrt{s} = 13$ TeV. Right: Cross section for $pp \to DD^c + X$ via two-gluon intermediate state at $\sqrt{s} = 13$ TeV.

function, which we take from the CTEQ14 NNLO set [145]. The middle panel of Fig. 4 shows $dL_{gg}/dM^2 = dL_{gg}/d\hat{s}$ for production of a state with mass $M = \sqrt{\hat{s}}$ in proton-proton collisions at $\sqrt{s} = 13$ TeV. This function behaves roughly as M^{-6} in the region of interest.

The relation between the gluon-gluon luminosity and the cross section for $\tilde{n}$ production in proton-proton collisions may be written as

$$\sigma(pp \to \tilde{n}X) = \frac{\pi^2}{8m_{\tilde{n}}}\Gamma(\tilde{n} \to gg)\left.\frac{dL_{gg}}{d\hat{s}}\right|_{\hat{s}=m_{\tilde{n}}^2}. \quad (35)$$

Assuming that the total width of $\tilde{n}$ is dominated by its two-gluon decay, this may then be used to calculate the cross section for $\tilde{n}$ production and decay to two photons:

$$\sigma(pp \to \tilde{n}X \to \gamma\gamma X) = \frac{\pi^2}{8m_{\tilde{n}}}\Gamma(\tilde{n} \to \gamma\gamma)\left.\frac{dL_{gg}}{d\hat{s}}\right|_{\hat{s}=m_{\tilde{n}}^2}. \quad (36)$$

We shall assume that the charged leptons L_i in the right-hand loop of Fig. 3 have the same masses as the D_i and that there are three families of them. We shall also assume that these masses are high enough above $m_{\tilde{n}}/2$ that the functions $F_{\pm}(\beta)$ may be approximated by 1. Then, adapting Eq. (9) of Ref. [134] to our assumptions, we find

$$\Gamma(\tilde{n} \to \gamma\gamma) = \left(\frac{\alpha}{3\pi}\right)^2 \frac{m_{\tilde{n}}^3}{16\pi\langle\tilde{n}\rangle^2}\left[3 \cdot 3 \cdot \left(-\frac{1}{3}\right)^2 + 3 \cdot (-1)^2\right]^2. \quad (37)$$

The first term in the square brackets is the contribution of the three D quarks, while the second term is the contribution of the three charged leptons L. There is an additional factor of 3 in the first term as the quarks are colored. The branching fraction $\mathcal{B}(\tilde{n} \to \gamma\gamma)$ is then approximately

$$\frac{\Gamma(\tilde{n} \to \gamma\gamma)}{\Gamma(\tilde{n} \to gg)} = \left(\frac{\alpha}{\alpha_s}\right)^2 \frac{8}{9} = 5.9 \times 10^{-3}. \quad (38)$$

(This value will be further reduced, possibly by as much as a factor of 2, by QCD corrections to the denominator.) Csaki and Randall obtain a similar value as they have similar contributions to the loop diagrams governing $\tilde{n} \to \gamma\gamma$ [130].

Combining Eqs. (36) and (37), we find

$$\sigma(pp \to \tilde{n}X \to \gamma\gamma X) = \frac{\alpha^2}{72\pi}\frac{m_{\tilde{n}}^2}{\langle\tilde{n}\rangle^2}\left.\frac{dL_{gg}}{d\hat{s}}\right|_{\hat{s}=m_{\tilde{n}}^2}. \quad (39)$$

Contours of equal $\sigma_0 \equiv \sigma(pp \to \tilde{n}X \to \gamma\gamma X)$ in the plane of $\langle\tilde{n}\rangle$ versus $m_{\tilde{n}}$ are easily plotted by solving Eq. (39) for $\langle\tilde{n}\rangle$:

$$\langle\tilde{n}\rangle = \alpha m_{\tilde{n}}\left(\frac{dL_{gg}/d\hat{s}}{72\pi\sigma_0}\right)^{1/2} \quad (40)$$

and varying $m_{\tilde{n}}$. The results for values of σ_0 between 0.01 and 10 fb are shown in Fig. 2, along with experimental limits from ATLAS [39] and CMS [41]. The vacuum expectation value $\langle\tilde{n}\rangle$ needed to produce a given cross section σ_0 varies roughly as $m_{\tilde{n}}^{-2}$ for the range shown.

VIII. THE ROLE OF A $\mathbb{Z}_2$ SYMMETRY IN NEUTRINO MIXING

The fundamental 27-plet of E_6 contains five neutral members, whose left-handed states we have denoted as $[\nu, N^c, L_1^0, L_2^{0c}, n]$ (cf. Table I, but omitting the family index i). In Ref. [15] we discussed a general 5×5 mass matrix in this basis space:

$$\mathcal{M}_5 = \begin{bmatrix} 0 & m_{12} & 0 & M_{14} & 0 \\ m_{12} & M_{22} & 0 & m_{24} & 0 \\ 0 & 0 & 0 & M_{34} & m_{35} \\ M_{14} & m_{24} & M_{34} & 0 & m_{45} \\ 0 & 0 & m_{35} & m_{45} & 0 \end{bmatrix}, \tag{41}$$

where masses with small letters correspond to $\Delta I_L = 1/2$ while those with capital letters correspond to $\Delta I_L = 0$. After diagonalization with respect to the third and fourth rows and columns, this becomes

$$\mathcal{M}_5' = \begin{bmatrix} 0 & m_{12} & M_{14}/\sqrt{2} & M_{14}/\sqrt{2} & 0 \\ m_{12} & M_{22} & m_{24}/\sqrt{2} & m_{24}/\sqrt{2} & 0 \\ M_{14}/\sqrt{2} & m_{24}/\sqrt{2} & M_{34} & 0 & (m_{35}+m_{45})/\sqrt{2} \\ M_{14}/\sqrt{2} & m_{24}/\sqrt{2} & 0 & -M_{34} & (m_{45}-m_{35})/\sqrt{2} \\ 0 & 0 & (m_{35}+m_{45})/\sqrt{2} & (m_{45}-m_{35})/\sqrt{2} & 0 \end{bmatrix}. \tag{42}$$

The first two rows and columns correspond to states with $\mathbb{Z}_2 = -1$, while the last three correspond to states with $\mathbb{Z}_2 = +1$. In the limit of exact $\mathbb{Z}_2$ symmetry, the parameters M_{14} and m_{24} vanish, so $\mathcal{M}_5'$ reduces to the direct sum of 2×2 and 3×3 matrices. The 2×2 matrix corresponds to the standard seesaw picture, with M_{22} taking on a large value to force SM neutrinos to have small masses $-m_{12}^2/M_{22}$. The 3×3 matrix has two large eigenvalues $\pm M_{34}$ (pseudo-Dirac $L_{1,2}^0$ states) and one small eigenvalue which we may identify as the n mass:

$$m_n = -2m_{35}m_{45}/M_{34}. \tag{43}$$

Here M_{34} may be as light as several hundred GeV, while m_{34} and m_{45} should be of the same order as SM quark and lepton masses. Thus the n states of each family should be lighter than the SM fermions in that family but could be considerably heavier than the corresponding neutrinos.

In Ref. [15] the states n were proposed as sterile neutrino candidates coupling to SM neutrinos through a violation of the $\mathbb{Z}_2$ symmetry, in order to explain various apparent anomalies in the three-active-neutrino picture. In the scenario in which $\mathbb{Z}_2$ is exact, however, a n state cannot account for the above-mentioned anomalies.

An exact $\mathbb{Z}_2$ symmetry could account for the existence of dark matter, in the form of the lightest state with $\mathbb{Z}_2 = -1$. The scalar $\tilde{\nu}$ or $\tilde{N}^c$ could be one such candidate. Other heavier states with $\mathbb{Z}_2 = -1$ could decay to it and one or several states with $\mathbb{Z}_2 = 1$. A full discussion of these possibilities is beyond the scope of the present paper, but some examples will be given in the next section.

IX. SIGNATURES FOR SO(10) 10-PLET FERMIONS

The decays of exotic quarks and leptons in the ten-dimensional representation of SO(10) depend crucially on whether the $\mathbb{Z}_2$ symmetry defined earlier is approximate or exact. We recall that singlets and 10-plets of SO(10) are assigned $\mathbb{Z}_2 = +1$ while 16-plets of SO(10) are assigned $\mathbb{Z}_2 = -1$. If $\langle\tilde{\nu}\rangle = \langle\tilde{N}\rangle = 0$, the $\mathbb{Z}_2$ is exact, while if one or both of these VEVs is nonvanishing, exotic 10-plets can mix with SM 16-plets.

A. Exotic quark production

Estimates of D pair production were made in Refs. [12,13], among many other places. We update those predictions for proton-proton collisions at the LHC center-of-mass (c.m.) energy of 13 TeV in the right panel of Fig. 4. If the scalar meson $\tilde{\nu}$ or $\tilde{N}^c$ is light enough, its exchange in the reaction $dd^c \to DD^c$ can provide an additional significant contribution to D pair production.

The only couplings that allow for the decay of an exotic D quark in the $\mathbb{Z}_2$-symmetry conserving way are the $\tilde{\nu}Dq_{d,s,b}$ and $\tilde{N}^cDq_{d,s,b}$ couplings. The inclusive searches for $2b$ jets plus missing transverse energy (MET) provide experimental lower bounds on the masses of these exotic quarks. Figure 5 shows the dominant diagrams for the production and decay of these exotic quarks that contribute to their experimental searches.

For these decays to be kinematically viable, we need $m_{\tilde{\nu}}$ and/or $m_{\tilde{N}^c}$ to be less than m_D. The ATLAS searches at 8 [146] and 13 TeV [147–149]; CMS searches [150] in run-1 data for third-generation squarks; and more recent CMS searches [151–154] put stringent lower bounds on the masses. Near the limit in which the difference between $m_{\tilde{\nu},\tilde{N}^c}$ and m_D is close to zero, the $2b$ jets plus MET searches are not sensitive. However, for exotic quark masses below 400 GeV, the monojet searches are sensitive in this limit, excluding exotic quarks in this region of parameter space.

For $m_D > 400$ GeV, a considerable region of the parameter space is allowed and grows with the mass of the exotic

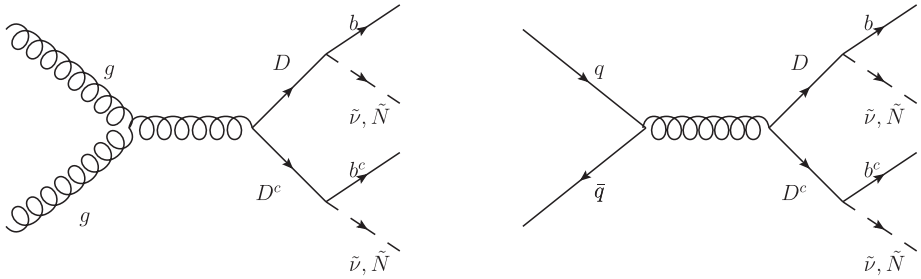

FIG. 5. Main diagrams contributing to $\mathbb{Z}_2$-preserving decays of exotic quark D.

quark. In order to estimate this difference, the 95% C.L. exclusion bound in [147], which is the most stringent bound on the sbottom searches, is recast. As the $gg \to D\bar{D}$ and $q\bar{q} \to D\bar{D}$ cross section is higher than the $gg \to \tilde{b}\,\tilde{\bar{b}}$ and $q\bar{q} \to b\tilde{\bar{b}}$ cross sections and as there are three copies of the exotic quarks, the production cross section of these quarks is greater than that of the sbottoms by about a factor of 20 near the electroweak and TeV scales. This results in more parameter space being excluded at 95% C.L. compared to the sbottom searches. We obtain results very close to such a recast performed in [155], which leads to an allowed mass difference of about 200 GeV between m_D and $m_{\tilde{\nu},\tilde{N}^c}$ at $m_D = 1$ TeV. For $m_D < 500$ GeV, a near degeneracy between m_D and $m_{\tilde{\nu},\tilde{N}^c}$ is required to escape jets plus MET searches. For $m_D < 400$ GeV, this degeneracy is not sufficient to evade the LHC searches as the monojet searches exclude the presence of exotic quarks in this limit.

As pointed out in [156], for small decay widths of the vectorlike quarks, quarkonium will form before the decay of the quark for an energy scale equal to twice the mass of the vectorlike quark. This quarkonium can then decay to produce a peak in the $\gamma\gamma$ spectrum at the mass twice that of the vectorlike quark. The cross section for this decay, $\sigma(pp \to DD^c \to \gamma\gamma)$, is proportional to N^2Q^4, where N is the number of generations and Q is the electric charge. As quoted in [156], this cross section is 10 fb for the bound state mass of 800 GeV with $N = 1$ and $Q = 5/3$ at $\sqrt{s} = 13$ TeV. In our model $N = 3$ and $Q = 1/3$, which results in the reduction of the cross section by a factor of ~70. Therefore, in our case, this cross section at the bound state mass of 800 GeV is ~0.14 fb and decreases exponentially with increasing bound state mass. As the lower bound on the exotic quarks in our model is ~400 GeV as allowed by the LHC searches described above, the lower bound on the quarkonium mass is ~800 GeV. Thus, in our model such a $\gamma\gamma$ peak due to a quarkonium bound state can only appear at higher energies for higher luminosities than those corresponding to the data analyzed up to August 2016.

In the limit of preserved $\mathbb{Z}_2$ symmetry, the region of parameter space for which $m_{\tilde{\nu},\tilde{N}^c} > m_D$ implies that the new exotic quarks are long-lived stable particles. These will be subject to R-hadron searches, stopped long-lived particle searches, and searches for disappearing tracks at both ATLAS [157–159] and CMS [160–163]. In particular, the ATLAS search [158] for full run-1 data excludes long-lived sbottoms for masses lower than 845 GeV.

Given that the production cross section for the exotic quarks in our model is about 20 times higher than the sbottom pair production in this region, the experimental lower bound on the exotic quark mass is well above 1 TeV. As shown in Fig. 2, the ATLAS [39] and CMS [41] searches in the diphoton channel put bounds on the vacuum expectation values of the $\tilde{n}$ field. The ATLAS bound [39] with 15.6 fb^{-1} (see [40] for an update) is the strongest for a low diphoton decay width of 4 MeV and corresponds to $\langle\tilde{n}\rangle = 700$ GeV for $m_{\tilde{n}} = 1$ TeV. Naive future projections assuming constant acceptance for higher luminosities can potentially raise this bound on the VEV to 1.4 TeV for an integrated LHC luminosity of 300 fb^{-1} and to about 2.5 TeV for 3000 fb^{-1}, if no diphoton resonance is discovered below 1 TeV. Thus, the inequality $m_{\tilde{\nu},\tilde{N}^c} > m_D$ can be viable for exotic quarks heavier than long-lived search bounds from the LHC.

Finally, the $\mathbb{Z}_2$ symmetry can be broken to allow mixing of the exotic quarks with the SM quarks. Let us assume that one such quark, called D_3, decays mainly via mixing with the b quark. Final-state branching ratios are then predicted to be $2:1:1$ for $Wt:Zb:Hb$, where H denotes the SM Higgs boson with mass 125 GeV [12], when the branching ratio for $D_3 \to b + m_{\tilde{\nu},\tilde{N}^c}$ is suppressed, which would be the case for $m_{\tilde{\nu},\tilde{N}^c} > m_D$. The most promising of these final states is probably Zb, where $Z \to e^+e^-$, $\mu^+\mu^-$, or $b\bar{b}$ (the last identified through b tagging).

Published LHC lower limits on m_D are of order 750 GeV at $\sqrt{s} = 8$ TeV. Specifically, ATLAS sets lower limits of 755 GeV in the mode $D_3 \to Zb$ [164] and 735 GeV in the mode $D_3 \to Hb$ [165]. The lower limits set by CMS [125] range between 740 and 900 GeV depending on the values of the branching fractions of D_3 to Wt, Zb, and Hb. For this case of branching ratios $2:1:1$, the lower bound on the D_3 mass is 790 GeV. (CMS also searches for vectorlike heavy quarks with charge $2/3$ [166].) A mass of 750 GeV corresponds to a cross section at 13 TeV of about 100 fb.

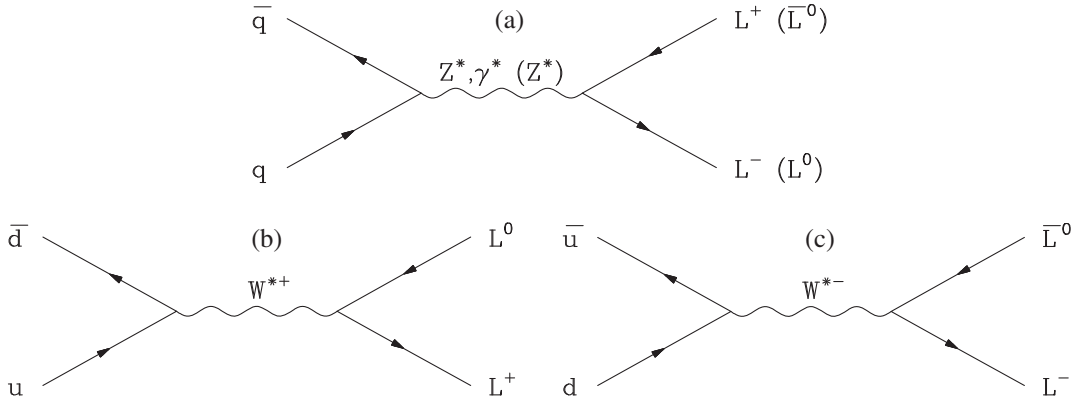

FIG. 6. Drell-Yan processes contributing to exotic lepton pair production via (a) virtual γ, Z^0; (b) virtual W^+; and (c) virtual W^-.

B. Exotic lepton production

The weak isodoublet vectorlike leptons L can be produced in pairs by the Drell-Yan process, illustrated in Fig. 6. Both a virtual photon (γ^*) and a virtual SM Z boson (Z^*) contribute to L^+L^- production; only Z^* contributes to $L^0\bar{L}^0$ production; and $W^{*\pm}$ contributes to L^+L^0 or $L^-\bar{L}^0$ production.

For Drell-Yan production of L^+L^- and $L^0\bar{L}^0$ [167], let M be the effective mass of the $L\bar{L}$ pair, y its pseudorapidity, and θ^* the angle between the outgoing lepton L and the incident quark q in the $q\bar{q}$ c.m. Let the proton with laboratory momentum $+p$ $(-p)$ emit a parton with momentum fraction x_A (x_B). Then for vectorlike $L\bar{L}$ production,

$$\frac{d\sigma(pp \to L\bar{L} + \ldots)}{dM dy d(\cos\theta^*)} = \frac{M x_A x_B}{48\pi}\left[\sum_q [f_q^A(x_A) f_{\bar{q}}^B(x_B) + f_{\bar{q}}^A(x_A) f_q^B(x_B)] S_q (1 + \cos^2\theta^*)\right], \tag{44}$$

where S_q, to be defined presently, incorporates the couplings of initial and final fermions to the virtual photon and Z. In general there would also be a term proportional to $\cos\theta^*$, but it is absent here because neither the charged nor the neutral L has an axial-vector coupling to the Z^0. Specifically, defining

$$\Delta_\alpha \equiv M^2 - M_\alpha^2, \qquad \gamma_\alpha \equiv M_\alpha \Gamma_\alpha, \qquad D_\alpha \equiv (\Delta_\alpha^2 + \gamma_\alpha^2)^{-1},$$
$$X_{\alpha\beta} \equiv D_\alpha D_\beta (\Delta_\alpha \Delta_\beta + \gamma_\alpha \gamma_\beta), \tag{45}$$

we have (with Greek letters standing for γ, Z^0)

$$S_q = \sum_{\alpha,\beta} X_{\alpha\beta} (C_V^{q,\alpha} C_V^{q,\beta} + C_A^{q,\alpha} C_A^{q,\beta})(C_V^{L,\alpha} C_V^{L,\beta} + C_A^{L,\alpha} C_A^{L,\beta}). \tag{46}$$

The vector and axial-vector couplings of the initial and final fermions are listed in Table IV, where $g_Z \equiv e/\sqrt{x(1-x)}$, $x \equiv \sin^2\theta_W$, and $-e$ is the electron charge. We consider only contributions of u, d, and s partons and antipartons in the proton. Integrating Eq. (44) over y, $\cos\theta^*$, and M, for the example of $M(L) = 400$ GeV, one finds

$$\sigma(pp \to L^+L^-X) = 12.4(13.6, 16.3)\ \text{fb},$$
$$\sigma(pp \to L^0L^0X) = 11.3(12.7, 15.7)\ \text{fb}, \tag{47}$$

where the first values are based on the above expressions. The second set are obtained using MADGRAPH [168], which has subroutines for production of charginos and neutralinos in the minimal supersymmetric standard model. The $L^\pm$ may be identified with Higgs-like charginos, while the neutral Ls may be identified with Higgs-like neutralinos. The third set, CERN Higgsino cross sections at 13 TeV [169], includes higher-order corrections ("K factors") which are seen to be relatively modest.

The formalism for production of charged exotic lepton pairs via virtual $W^\pm$ is similar. We list the relevant coupling constants in Table V. Here $g_W = e/\sqrt{x}$. The predicted cross sections for $L\bar{L}$ production at 13 TeV are shown in Fig. 7. (We believe the cross sections for charged exotic pairs given in Ref. [169] are high by a factor of 2.)

Decays of charged and neutral L's are problematic. The heavier is likely to decay via beta decay to the lighter unless their masses are very close to one another. The lighter is likely to decay via mixing with a light lepton if $\mathbb{Z}_2$ symmetry is broken by a small VEV of $\tilde{\nu}_e$ or $\tilde{n}^c$ (see Table II). Thus, if the neutral L is lighter, we will have such

TABLE V. Vector and axial-vector couplings of fermions for L^+L^0 and $L^-\bar{L}^0$ Drell-Yan production via $W^{*\pm}$.

$u\bar{d}$		$d\bar{u}$		L^+L^0	$L^-\bar{L}^0$
C_V	C_A	C_V	C_A	C_V	C_V
$\sqrt{2}g_W/4$	$-\sqrt{2}g_W/4$	$\sqrt{2}g_W/4$	$-\sqrt{2}g_W/4$	$\sqrt{2}g_W/2$	$\sqrt{2}g_W/2$

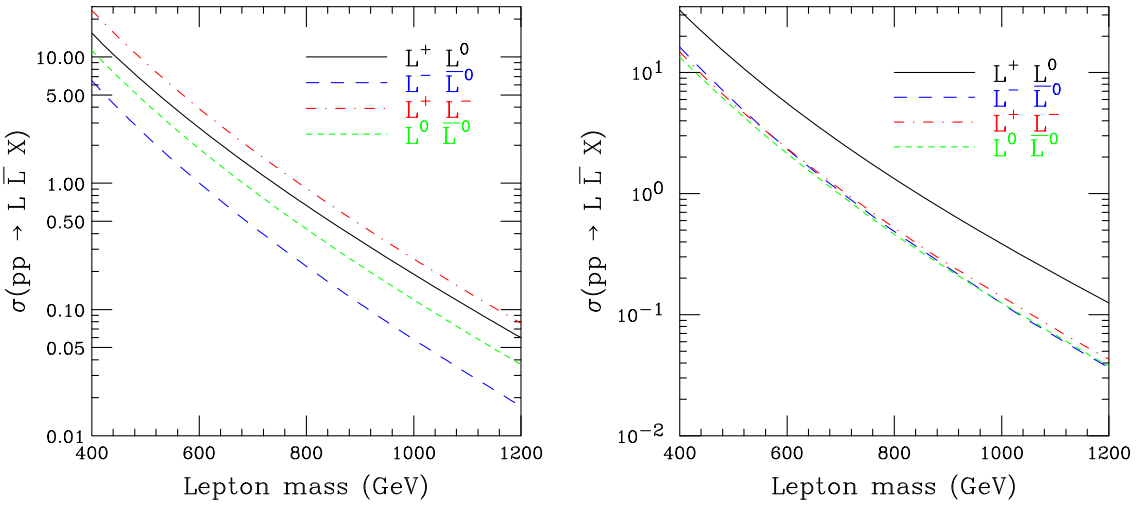

FIG. 7. Predicted cross sections in femtobarns for production of $L\bar{L}$ pairs by proton-proton collisions at $\sqrt{s} = 13$ TeV. Left: Leading-order; right: calculation for Higgsinos using MADGRAPH [168].

processes as $L^0 \to \ell_i^- W^+$ and $L^0 \to \nu_i Z^0$, while if the charged L is lighter, we will have, e.g., $L^- \to \ell_i^- Z^0$ and $L^- \to W^- \nu_i$. Here $\ell_i^- = (e^-, \mu^-, \tau^-)$ and $\nu_i = (\nu_e, \nu_\mu, \nu_\tau)$. If the $\mathbb{Z}_2$ symmetry is exact, the charged and neutral L's will decay to a $\tilde{\nu}$ or a $\tilde{n}$ and a SM lepton if kinematically allowed.

The sensitivities of searches for charged and neutral leptons L are highly dependent on their decay modes, in which mixing with the light charged and neutral leptons plays a key role. (See, e.g., [12].) Limits are given by ATLAS [170–174] and CMS [175–178] at $\sqrt{s} = 8$ TeV and by CMS [179] at 13 TeV. The value $M(L^\pm) = 400$ GeV which we have quoted above is near the allowed lower limit [83]; lower limits on heavy exotic quark masses are typically twice as large. The associated production reactions $pp \to (L^- \bar{L}^0, L^+ L^0) + X$ via virtual W exchange are a promising way of producing the exotic heavy leptons [83]. Searches should bear in mind the possibility that the exotic leptons of all three fermion 27-plets may have masses in the several-hundred-GeV range, giving rise to peaks in $Z\ell$ and $W\ell$ mass distributions.

C. Sterile neutrinos $n_{1,2,3}$

A recent treatment of sterile neutrinos within the context of E_6 was given in Ref. [15]. At most two such neutrinos are assigned masses in the eV range to improve fits to oscillations and possible depletions of reactor fluxes. This leaves one or two of the n_i to acquire higher masses, possibly in the keV range as a dark matter candidate to account for depletion of small-scale structure of the Universe [180–183] or for a weak gamma-ray line at 3.5 keV stemming from decay of a 7 keV neutrino [184,185]. We shall not discuss the pros and cons of such an assignment here (see [186] for a thorough treatment), as we are concerned mainly with hadron collider signatures.

In this context one may note that through imposition of a discrete $\mathbb{Z}_2$ symmetry suppressing the VEVs of the neutral SO(10) 16-plets $\tilde{\nu}$ and $\tilde{N}^c$, an n mass may be generated entirely through mixing with the exotic leptons L^0 and $\bar{L}^0$ [15], and so in principle can be large, even reaching the TeV scale. Such mixing would affect the decay schemes of charged and neutral leptons L.

X. DIAGNOSTICS FOR EXTRA Z BOSONS

Many grand unified theories can have neutral gauge bosons heavier than the Z^0 but still accessible at present hadron collider energies [10,187,188]. We update a discussion regarding their identification. It was shown in Refs. [8,9,167,189,190] that a good diagnostic tool for determining the nature of any Z is the forward-backward asymmetry of the lepton pairs to which it decays. In a proton-antiproton collider a nonzero asymmetry can occur for lepton pairs integrated over the rapidity y of their c.m. For a proton-antiproton collider, this asymmetry is an odd function of rapidity, so it must be displayed as a function of y.

The Z_N is that linear combination $Z_N = -(\sqrt{15}/4)Z_\psi - (1/4)Z_\chi$ [cf. Eq. (2)] to which left-handed antineutrinos do not couple. Consequently, they do not contribute to a triangle anomaly involving the Z_N and hence are free to acquire large Majorana masses. The forward-backward asymmetries for a number of different Z''s with masses 3 and 4 TeV at $\sqrt{s} = 13$ TeV are displayed in Fig. 8. The Z_ψ has purely axial-vector couplings to SM particles, explaining the absence of its asymmetry. While the Z_N contains much more Z_ψ than Z_χ, it does exhibit some asymmetry, about equal in magnitude and opposite in sign to that of a Z with SM couplings. The asymmetries for $M(Z') = 4$ TeV have nearly the same shape as those for $M(Z') = 3$ TeV but in a compressed range of y.

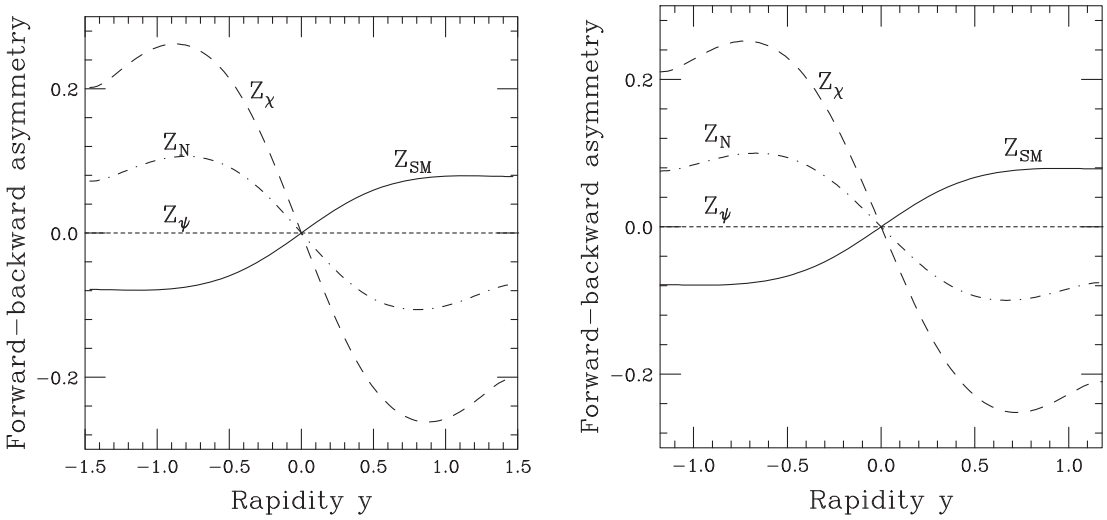

FIG. 8. Forward-backward asymmetries for several different Z's of mass 3 (left) and 4 (right) TeV.

To calculate forward-backward asymmetries $A_{\rm FB}$ in leptonic decays of a Z one needs quark distribution functions $q(x) \equiv x f_q(x)$ and left- and right-handed couplings to the Z for quarks and leptons. We consider only u and d quarks (s quarks contribute at most a few percent to cross sections and asymmetries). Let the right-moving proton contribute a parton with momentum fraction x_1, while the left-moving proton contributes a parton with momentum fraction x_2. These are related to the rapidity y of the parton-parton c.m. (which is also the final dilepton c.m. rapidity) by

$$x_1 = \sqrt{\hat{s}/s}e^{y}, \qquad x_2 = \sqrt{\hat{s}/s}e^{-y}, \tag{48}$$

where $\hat{s}$ is the square of the effective mass of the parton-parton or dilepton system. (We neglect transverse momenta.) Then $A_{\rm FB} = \sigma_{F-B}/\sigma_{F+B}$, where

$$\sigma_{F-B} = C\{[(u(x_1)\bar{u}(x_2) - u(x_2)\bar{u}(x_1)][L_u^2 - R_u^2] \times [L_\ell^2 - R_\ell^2] + (u \to d)\}, \tag{49}$$

$$\sigma_{F+B} = C\{[(u(x_1)\bar{u}(x_2) + u(x_2)\bar{u}(x_1)][L_u^2 + R_u^2] \times [L_\ell^2 + R_\ell^2] + (u \to d)\}, \tag{50}$$

with C a common constant and L, R denoting left- and right-handed couplings, respectively. Only the ratios of these couplings are important, so we quote them without normalization. The couplings are shown in Table VI; we take $x = 0.2315$. For the Z_ψ, Z_χ, and Z_N we use the charges in Table I, with suitable sign changes $Q(f_R) = -Q(f_L^c)$.

A sufficiently heavy Z_N can decay to all the pairs listed in Table I, diluting its branching fraction to SM particles and eroding the lower bounds on its mass. For example, whereas ATLAS places a 95% confidence-level lower limit of 4.05 TeV on the mass of a SM Z' based on 13.3 fb^{-1} at 13 TeV [109], and correspondingly weaker bounds for Z_χ and Z_ψ, these bounds assume only decays to SM particles. The same assumption is made by CMS in placing a lower bound of 4.0 TeV on the mass of Z' [110]. Suppose all channels in Table I are open (including right-handed neutrinos). Then the fraction r of decays to pairs of the SO(10) 16-plet for a $Z(\theta) \equiv Z_\psi \cos\theta + Z_\chi \sin\theta$ takes the form $r = (2/9) + (2/9)\sin^2\theta$, i.e., $(2/9) \le r \le (4/9)$. The exotic SO(10) 10-plet and singlet members thus can affect the reach of Z' searches. The mass of Z' and a way to escape the search bounds for the current model are discussed in Sec. IV.

XI. FUTURE PROJECTIONS

In the previous sections, we discussed the detection signatures and properties of the electroweak and TeV scale fermions, scalars, and vectors bosons, as well as the individual constraints on their masses. The next pertinent question is how the discovery or nondiscovery of any one type of the above will affect the constraints on the mass spectra of the other types. Another question is whether such a discovery will exclude the model in some parameter region. In the following, we quantify these questions for the minimal scenario of three fermion and one scalar generation of 27-plets of E_6 in the matter sector.

TABLE VI. Left- and right-handed couplings of u quarks, d quarks, and SM charged leptons ℓ to various Z's.

Z type	L_u	R_u	L_d	R_d	L_ℓ	R_ℓ
SM	$\frac{1}{2} - \frac{2}{3}x$	$-\frac{2}{3}x$	$-\frac{1}{2} + \frac{1}{3}x$	$\frac{1}{3}x$	$-\frac{1}{2} + x$	x
Z_χ	-1	1	-1	-3	3	1
Z_ψ	1	-1	1	-1	1	-1
Z_N	-1	1	-1	2	-2	1

Discovery of a $\gamma\gamma$ resonance will fix the mass and the cross section, which will fix the value of $\langle\tilde{n}\rangle$ in this model according to Eq. (40). Therefore, Eq. (21) would determine the value of b_{17}. Figure 2 can be used to put bounds on the allowed Yukawa couplings for the exotic quarks and leptons.

In the left panel of Fig. 9, the [red] dashed contours show the minimum value of b_{17} required to avoid an unstable potential. As expected, it increases with increasing Yukawa coupling because Yukawa contributions y to the RGE of b_{17} are proportional to $-y^4$. After choosing a point in this plane, the [red] dashed contour value at that point tells the minimum b_{17} necessary for the stability at that point. In order to calculate the upper bound of allowed b_{17} at that point, we need the difference between the upper and lower bounds. That difference is given by the [color or] position of the shaded region. For example, the inner [orange] region corresponds to the difference between the allowed upper and lower bound of at least 0.8. Similarly the middle [yellow] region implies that the allowed values of b_{17} are 0.5 to 0.8 more than the minimum values required by the stability condition as indicated by the [red] dashed contour. Finally in the outer [green] region the difference between the allowed upper and lower bounds on b_{17} can vary between 0.1 to 0.5.

Thus discovery of a $\gamma\gamma$ resonance will lead to fixing of b_{17} which can be readily used to fix the upper and lower bounds on fermion masses using the left panel of Fig. 9. Calculations leading to this figure forbid Yukawa values above 1.3, putting a tight upper bound on the fermion discovery.

If a Z_N is discovered before the rest of the spectrum, the constraint is reversed implying a very high value of $\langle\tilde{n}\rangle$, thus fixing the rest of the mass spectrum at a similar scale. In the right panel of Fig. 9, the boundary of the shaded [light blue] region corresponds to the minimum value of b_{17} allowed by stability conditions thus excluding the shaded [light blue] region left of this line. Therefore, a Z_N discovery will put a lower bound on the mass of the scalar $\tilde{n}$. As m_{Z_N} essentially fixes $\langle\tilde{n}\rangle$, each point in the $m_{Z_N} - m_{\gamma\gamma}$ space has a fixed value of allowed b_{17}, which can be used to bound the fermion masses using the left panel of Fig. 9. These upper bounds on the fermion masses are shown in the right panel of Fig. 9 with [red] solid contours for exotic quarks and [green] dashed contours for exotic leptons. Contour labels indicate the masses of fermions in TeV. Thus the masses of Z_N and $\gamma\gamma$ resonances can fix an upper bound on the fermion masses, leading to exclusion of the minimal scenario if a heavier fermion is discovered.

If an exotic fermion with mass M is discovered first, that will introduce a lower bound on the value of $\langle\tilde{n}\rangle$ of about M due to the upper bound on the Yukawa couplings of 1.3. This will set a lower bound on the mass of Z_N and a corresponding lower bound on the mass of an observable $\gamma\gamma$ resonance. Discovery of either of these below these bounds will exclude this minimal scenario. The model can be rescued by adding another generation of scalars, which has

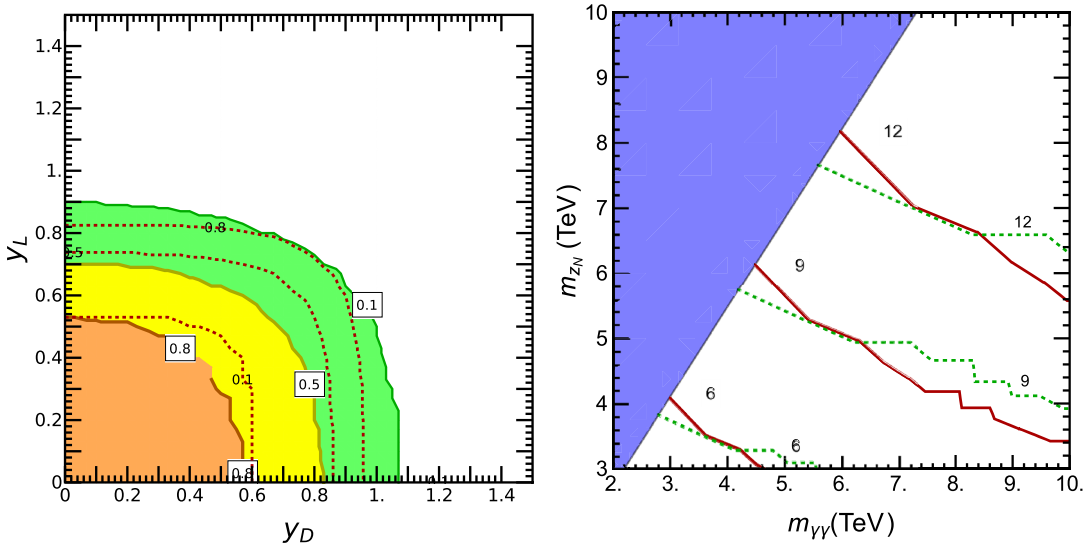

FIG. 9. Left: Dashed [red] contours correspond to minimum required value of b_{17} for stability. Shaded [colored] backgrounds with boundaries labeled by boxed numbers indicate the total range of b_{17} values, i.e., the difference between maximum and minimum values of b_{17} allowed at that point. The inner [orange] region corresponds to the range of at least 0.8 above the minimum value given by the [red] dashed contour. The middle [yellow] region implies that the allowed b_{17} values are 0.5 to 0.8 more than the minimum values required by the stability condition as indicated by the [red] dashed contour. The outer [green] region denotes the corresponding range of 0.1 to 0.5. Right: Shaded [light blue] region excluded by stability constraints. Solid [red] contours indicate maximum exotic quark mass allowed in TeV. Dashed [green] contours indicate maximum exotic lepton mass allowed in TeV.

a required SO(10) singlet to give a mass to the Z_N boson, thus decoupling it from the rest of the constraints.

Fortunately, searches at the LHC continue to progress, as exemplified by the recent ATLAS [40,112,148,149] and CMS [151–154] results quoted here. In the absence of a new discovery, Fig. 2 also shows the dashed [red] contours with labels indicating the integrated luminosities at the LHC. The regions to the left of these type of contours are excluded, if the LHC run up to the indicated luminosity does not find any $\gamma\gamma$ resonance. The remaining viable parameter space can be further reduced using the lower bounds on $\langle\tilde{n}\rangle$ coming from the nondiscovery of a Z_N boson and exotic fermions.

XII. CONCLUSIONS

We have discussed some signatures for TeV-scale physics and for dark matter candidates of an E_6 scheme. One prediction of this framework is the existence of a weak isosinglet scalar particle $\tilde{n}$ belonging to the same 27-plet as the SM Higgs boson. This picture necessarily requires there to be a second Higgs boson (not discussed further here) as in all other two-Higgs-doublet models. The E_6 scheme entails a number of predictions testable in continued LHC operation at $\sqrt{s} = 13$ TeV. These include exotic weak isosinglet vectorlike quarks "D" with charges $\mp 1/3$, and exotic weak isodoublet leptons L_1^-, L_1^0, L_2^{0c}, and L_2^+. The quarks and leptons should have masses at the TeV scale if those masses are generated by the VEV of $\tilde{n}$. Suggestions for observing them at the LHC have been made. There should be a several-TeV-scale Z_N (not coupling to right-handed neutrinos) whose leptonic decays should exhibit a characteristic forward-backward asymmetry, odd in rapidity of the dilepton system.

The branching ratios of $\tilde{n}$ to $\gamma\gamma$, $Z\gamma$, ZZ, and WW should be in definite ratios $1:0.24:2.08:5.32$, affording the possibility of early confirmation or refutation of the model. We also demonstrated how the discovery of any of the exotic fermions, bosons or scalar in the minimal scenario of three fermion generations and a scalar generation can tightly constrain the rest of the mass spectrum and exclude or strengthen the evidence for an E_6 scenario based on a subsequent discovery.

ACKNOWLEDGMENTS

We thank Carl Albright, Jun Gao, Sam Harper, Boaz Klima, Joe Lykken, Petra Merkel, Pavel Nadolsky, Jim Pilcher, Chris Quigg, Michael Ratz, Tom Rizzo, Lian-Tao Wang, and Carlos Wagner for helpful comments. This work was supported in part by the United States Department of Energy through Grant No. DE FG02 13ER41958. A. J. thanks Michael Ramsey-Musolf at the Amherst Center for Fundamental Interactions (ACFI) for hospitality and support during a portion of this work. The work done while at ACFI was supported in part by the U.S. Department of Energy under contract DE-SC0011095. J. L. R. thanks the Mainz Institute for Theoretical Physics (MITP), the Università di Napoli Federico II, and INFN for its hospitality and its partial support during a portion of this work. MITP is part of the Excellence Cluster PRISMA (EXC 1098) funded by the German Research Foundation (Deutsche Forschungsgemeinschaft).

APPENDIX A: DECOMPOSITION OF 27-PLET, 78-PLET AND 351′-PLET

The decomposition of the 27-plet, 78-plet and 351′-plet into the components invariant under lower-ranked symmetry groups is shown below [105]. $U(1)_\psi$ charges are noted in square brackets, $U(1)_\chi$ charges in the brackets, and $U(1)_N$ charges in parentheses.

First, $E_6 \to SO(10) \times U(1)_\psi$ breaking leads to the following decomposition of the E_6-invariant multiplets:

$$\begin{aligned} 27 &= 1[4] + 10[-2] + 16[1], \\ 78 &= 1[0] + 16[-3] + \overline{16}[3] + 45[0], \\ 351' &= 1[-8] + 10[-2] + \overline{16}[-5] + 54[4] \\ &\quad + \overline{126}[-2] + 144[1]. \end{aligned} \tag{A1}$$

Next, $SO(10) \times U(1)_\psi \to SU(5) \times U(1)_\chi \times U(1)_\psi$ breaking leads to the decomposition of the SO(10) invariant multiplets. The original E_6-invariant multiplets can now be written as the following $U(1)_\psi \times SU(5) \times U(1)_\chi$ components:

$$\begin{aligned} 27 &= [4]1\{0\} + [-2]5\{2\} + [-2]\bar{5}\{-2\} + [1]1\{-5\} + [1]\bar{5}\{3\} + [1]10\{-1\}, \\ 78 &= [0]1\{0\} + [-3]1\{-5\} + [-3]\bar{5}\{3\} + [-3]10\{-1\} + [3]\bar{1}\{5\} + [3]5\{-3\} + [3]\overline{10}\{1\} \\ &\quad + [0]1\{0\} + [0]10\{4\} + [0]\overline{10}\{-4\} + [0]24\{0\}, \\ 351' &= [-8]1\{0\} + [-2]5\{2\} + [-2]\bar{5}\{-2\} + [-5]\bar{1}\{5\} + [-5]5\{-3\} + [-5]\overline{10}\{1\} \\ &\quad + [4]15\{4\} + [4]\overline{15}\{-4\} + [4]24\{0\} + [-2]\bar{1}\{10\} + [-2]5\{2\} + [-2]\overline{10}\{6\} + [-2]15\{-6\} + [-2]\overline{45}\{-2\} \\ &\quad + [-2]45\{2\} + [1]\bar{5}\{3\} + [1]5\{7\} + [1]10\{-1\} + [1]15\{-1\} + [1]24\{-5\} + [1]40\{-1\} + [1]\overline{45}\{3\}. \end{aligned} \tag{A2}$$

Finally, $SU(5) \times U(1)_\chi \times U(1)_\psi \to SU(5) \times U(1)_N$ results in the following charge allocations:

TABLE VII. Members of 27-plet of E_6, their SO(10) and SU(5) representations, and their U(1) charges. The weak hypercharge Y_W is equal to $2(Q - I_{3L})$. Mass scale refers to scalar members. MTeV = multi-TeV.

SO(10), SU(5)	$2\sqrt{6}Q_\psi$	$2\sqrt{10}Q_\chi$	$2\sqrt{10}Q_N$	$SU(3)_c$	$SU(2)_L$	Y_W	Mass scale
$16, \bar{5}$	1	3	−2	$\bar{3}$	1	2/3	GUT
				1	2	−1	TeV
16, 10		−1	−1	$\bar{3}$	1	−4/3	GUT
				3	2	1/3	GUT
				1	1	2	GUT
16, 1		−5	0	1	1	0	TeV
$10, \bar{5}$	−2	−2	3	$\bar{3}$	1	2/3	GUT
				1	2	−1	EW/TeV
10, 5		2	2	3	1	−2/3	GUT
				1	2	1	EW/TeV
1, 1	4	0	−5	1	1	0	TeV/MTeV

TABLE VIII. Members of 78-plet of E_6, their SO(10) and SU(5) representations, and their U(1) charges. The weak hypercharge Y_W is equal to $2(Q - I_{3L})$. Masses are at GUT scale for all scalar members. SU(5) singlets in 16 and $\overline{16}$ of SO(10) do not get VEVs in order to preserve the $U(1)_N$ down to multi-TeV scale.

SO(10), SU(5)	$2\sqrt{6}Q_\psi$	$2\sqrt{10}Q_\chi$	$2\sqrt{10}Q_N$	$SU(3)_c$	$SU(2)_L$	Y_W
45, 24	0	0	0	8	1	0
				1	3	0
				3	2	−5/3
				$\bar{3}$	2	5/3
				1	1	0
45, 10		4	−1	3	2	1/3
				$\bar{3}$	1	−4/3
				1	1	2
$45, \overline{10}$		−4	1	$\bar{3}$	2	−1/3
				3	1	4/3
				1	1	−2
45, 1		0	0	1	1	0
$16, \bar{5}$	−3	3	3	$\bar{3}$	1	2/3
				1	2	−1
16, 10		−1	4	$\bar{3}$	1	−4/3
				3	2	1/3
				1	1	2
16, 1		−5	5	1	1	0
$\overline{16}$,5	3	−3	−3	3	1	−2/3
				1	2	1
$\overline{16}, \overline{10}$		1	−4	3	1	4/3
				$\bar{3}$	2	−1/3
				1	1	−2
$\overline{16}, 1$		5	−5	1	1	0
1, 1	0	0	0	1	1	0

TABLE IX. Members of $351'$-plet of E_6, their SO(10) and SU(5) representations, and their U(1) charges. The weak hypercharge Y_W is equal to $2(Q - I_{3L})$. Masses are at GUT scale for all the members.

SO(10), SU(5)	$2\sqrt{6}Q_\psi$	$2\sqrt{10}Q_\chi$	$2\sqrt{10}Q_N$	$SU(3)_c$	$SU(2)_L$	Y_W
$144, \overline{45}$	1	3	−2	8	2	−1
				6	1	2/3
				3	2	7/3
				3	1	−8/3
				$\bar{3}$	3	2/3
				$\bar{3}$	1	2/3
				1	2	−1
144, 40		−1	−1	$\bar{6}$	2	1/3
				8	1	2
				$\bar{3}$	3	−4/3
				$\bar{3}$	1	−4/3
				3	2	1/3
				1	2	−3
144, 24		−5	0	8	1	0
				3	2	−5/3
				$\bar{3}$	2	5/3
				1	3	0
				1	1	0
144, 15		−1	−1	6	1	−4/3
				3	2	1/3
				1	3	2
144, 10		−1	−1	3	2	1/3
				$\bar{3}$	1	−4/3
				1	1	2
144, 5		7	−3	3	1	−2/3
				1	2	1
$144, \bar{5}$		3	−2	$\bar{3}$	1	2/3
				1	2	−1

TABLE X. Members (contd.) of 351′-plet of E_6, their SO(10) and SU(5) representations, and their U(1) charges. Masses are at GUT scale for all the members.

SO(10), SU(5)	$2\sqrt{6}Q_\psi$	$2\sqrt{10}Q_\chi$	$2\sqrt{10}Q_N$	$SU(3)_c$	$SU(2)_L$	Y_W
$\overline{126}, 50$	−2	2	2	8	2	1
				6	1	8/3
				$\bar{6}$	3	−2/3
				$\bar{3}$	2	−7/3
				3	1	−2/3
				1	1	−4
$\overline{126}, \overline{45}$		−2	3	8	2	−1
				6	1	2/3
				3	2	7/3
				3	1	−8/3
				$\bar{3}$	3	2/3
				$\bar{3}$	1	2/3
				1	2	−1
$\overline{126}, 15$		−6	4	6	1	−4/3
				3	2	1/3
				1	3	2
$\overline{126}, \overline{10}$		6	1	$\bar{3}$	2	−1/3
				3	1	4/3
				1	1	−2
$\overline{126}, 5$		2	2	3	1	−2/3
				1	2	1
$\overline{126}, 1$		10	0	1	1	0

$$
\begin{aligned}
27 &= 1(-5) + 5(2) + \bar{5}(3) + 1(0) + \bar{5}(-2) + 10(-1),\\
78 &= 1(0) + 1(5) + \bar{5}(3) + 10(4) + \bar{1}(-5) + 5(-3) + \overline{10}(-4) + 1(0) + 10(-1) + \overline{10}(1) + 24(0),\\
351' &= 1(10) + 5(2) + \bar{5}(3) + \bar{1}(5) + 5(7) + \overline{10}(6) + 15(-6) + \overline{15}(-4) + 24(-5) + \bar{1}(0) + 5(2) + \overline{10}(1) + 15(4)\\
&\quad + \overline{45}(3) + 50(2) + \bar{5}(-2) + 5(-3) + 10(-1) + 15(-1) + 24(0) + 40(-1) + \overline{45}(-2). \qquad \text{(A3)}
\end{aligned}
$$

These results are summarized in Tables VII–XI.

APPENDIX B: DETAILS OF (PSEUDO)SCALAR POTENTIALS

For the case of $a = 0$ and a new pseudoscalar as the Goldstone boson of $U(1)_N$, from Eq. (13) we get

$$b_{15}v_d^2 + b_{14}v_u^2 + b_3\langle\tilde{n}\rangle^2 + m_3^2 = 0, \qquad \text{(B1)}$$

$$b_{14}v_d^2 + b_{16}v_u^2 + b_4\langle\tilde{n}\rangle^2 + m_4^2 = m_A^2, \qquad \text{(B2)}$$

$$b_3 {v_d}^2 + b_4 {v_u}^2 + b_{17}\langle\tilde{n}\rangle^2 + m_5^2 = 0. \qquad \text{(B3)}$$

Substituting these back in Eq. (11), we get

$$\mathcal{M}_{Ln}^s = \begin{pmatrix} 2b_{15}v_d^2 & 2b_{14}v_u v_d & 2b_3 v_d\langle\tilde{n}\rangle \\ 2b_{14}v_u v_d & 2b_{16}v_u^2 + m_A^2 & 2b_4 v_u\langle\tilde{n}\rangle \\ 2b_3 v_d\langle\tilde{n}\rangle & 2b_4 v_u\langle\tilde{n}\rangle & 2b_{17}\langle\tilde{n}\rangle^2 \end{pmatrix}. \qquad \text{(B4)}$$

This structure implies that the strength of mixing between singlet and doublet is proportional to b_3, b_4 and $\langle\tilde{n}\rangle$. For a scalar (not pseudoscalar) $\tilde{n}$, the small mixing then would imply

$$b_{17} \sim \frac{m_{\tilde{n}}^2}{2\langle\tilde{n}\rangle^2}. \qquad \text{(B5)}$$

For $m_{\tilde{n}} \sim \mathcal{O}(\text{TeV})$ this would make $b_{17} \sim 1$, requiring b_3 and b_4 to be constrained to limit the mixing. Making the spinless candidate a pseudoscalar by adding another scalar, this term in the mass matrix becomes $m_{\tilde{n}}^2 + 2b_{17}\langle\tilde{n}\rangle^2$. In addition, b_{17} is now free to take on higher values leading to

TABLE XI. Members (contd.) of the 351′-plet of E_6, their SO(10) and SU(5) representations, and their U(1) charges. SU(2) triplet and SU(3) octet are contained in 54 of SO(10), while diquarks are contained in 54 of SO(10) and $\overline{16}$ of SO(10) as indicated below with mass scale marked as MTeV. SM singlets in (54, 24) and $(\overline{16}, 1)$ cannot get VEVs in order to preserve $U(1)_N$ symmetry down to the MTeV scale.

SO(10), SU(5)	$2\sqrt{6}Q_\psi$	$2\sqrt{10}Q_\chi$	$2\sqrt{10}Q_N$	$SU(3)_c$	$SU(2)_L$	Y_W	Mass scale
54, 15	4	4	−6	6	1	−4/3	GUT
				3	2	1/3	MTeV[a]
				1	3	2	GUT
$54, \overline{15}$		−4	−4	$\bar{6}$	1	4/3	GUT
				$\bar{3}$	2	−1/3	GUT
				1	3	−2	GUT
54, 24		0	−5	8	1	0	MTeV[b]
				3	2	−5/3	GUT
				$\bar{3}$	2	5/3	GUT
				1	3	0	MTeV[c]
				1	1	0	GUT
$\overline{16}, \overline{10}$	−5	1	6	$\bar{3}$	2	−1/3	MTeV[a]
				3	1	4/3	GUT
				1	1	−2	GUT
$\overline{16}$,5		−3	7	3	1	−2/3	GUT
				1	2	1	GUT
$\overline{16}$,1		5	5	1	1	0	GUT
$10, \bar{5}$	−2	−2	3	$\bar{3}$	1	2/3	GUT
				1	2	−1	GUT
10, 5		2	2	3	1	−2/3	GUT
				1	2	1	GUT
1, 1	−8	0	10	1	1	0	MTeV[d]

[a]Diquark.
[b]Color SU(3) octet.
[c]Weak SU(2) triplet.
[d]SO(10) singlet.

decoupling of the singlet and relaxation of the constraints on b_3 and b_4.

APPENDIX C: DETAILS OF RENORMALIZATION GROUP EVOLUTION AND UNIFICATION

1. Gauge couplings

The model has $U(1)_Y \times SU(2)_L \times SU(3)_c \times U(1)_N$ symmetry at the TeV scale before spontaneous breaking. The one-loop RG equations corresponding to the gauge coupling constants (g_i) are [191]

$$\frac{d\alpha_i^{-1}}{dt} = -\frac{b_i}{2\pi}, \tag{C1}$$

where $\alpha_i = \frac{g_i^2}{4\pi}$, $t = \log(\Lambda/\mathrm{GeV})$.

For the SM, we have

$$b_1 = \frac{41}{10}, \qquad b_2 = -\frac{19}{6}, \qquad b_3 = -7. \tag{C2}$$

In the E_6 model with N_f generations of fermions and N_s generations of scalars of 27-plets, we obtain

$$b_1 = 2\left(N_f + \frac{N_s}{2}\right), \qquad b_2 = 2\left(N_f + \frac{N_s}{2}\right) - \frac{22}{3},$$
$$b_3 = 2\left(N_f + \frac{N_s}{2}\right) - 11, \qquad b_N = 2\left(N_f + \frac{N_s}{2}\right). \tag{C3}$$

The scalar 27-plet generation contributes half of that of a fermion generation, as it has half the number of degrees of freedom compared to a Weyl fermion. The above values take into account the full scalar generation. In order to avoid violation of proton decay bounds, we set the colored scalar masses $> 10^{16}$ GeV for the 27-plet scalar generation. All of the 78-plet scalar resides at the GUT scale so it does not contribute to the low-energy evolution of the gauge couplings. For the 351′-plet scalar, as described in Sec. II and Appendix A, two copies of diquark, an SU(2) triplet, an SU(3) octet, and an SO(10) singlet reside at the MTeV scale as indicated in Table XI of Appendix A.

In making Fig. 10, for simplicity, we assume that all of the 27-plet exotic fermions and low-energy components of the 27-plet scalar marked with mass scale other than GUT in Table VII are below or close to 1 TeV so we include those in the running of the couplings from 1 to 10 TeV. That gives

$$b_1 = \left(2N_f + \frac{3}{10}\right) = \frac{63}{10}, \quad b_2 = \left(2N_f - \frac{22}{3} + \frac{1}{2}\right) = -\frac{5}{6},$$
$$b_3 = (2N_f - 11) = -5, \quad b_N = \left(2N_f + \frac{59}{120}\right) = \frac{779}{120}. \tag{C4}$$

The rest of the low-energy states are assumed to reside above 1 TeV but below or around 10 TeV marked as the MTeV mass scale in Table XI in making Fig. 10. Under the above conditions, the one-loop beta functions for the evolution from 10 TeV to the GUT scale are given as

$$b_1 = \left(2N_f + \frac{3}{10} + 2\left(\frac{1}{30}\right)\right) = \frac{191}{30},$$
$$b_2 = \left(2N_f - \frac{22}{3} + \frac{1}{2} + 2\left(\frac{1}{2}\right) + \frac{2}{3}\right) = \frac{5}{6},$$
$$b_3 = \left(2N_f - 11 + 2\left(\frac{1}{3}\right) + 1\right) = -\frac{10}{3},$$
$$b_N = \left(2N_f + \frac{59}{120} + 2\left(\frac{9}{5}\right) + \frac{55}{24} + \frac{5}{6}\right) = \frac{793}{60}. \tag{C5}$$

Figure 10 shows the SM gauge RG evolution along with that for the current model where red (second from the top solid), green (third from the top solid) and blue (lower-most solid) lines correspond to $U(1)_Y$, $SU(2)_L$, and $SU(3)_c$, respectively. The black (uppermost solid) line corresponds to $U(1)_N$ evolution. It is evolved to lower energies starting from the unification point. Its intersection with the lower bound on the Z_N mass is used in Sec. IV to derive a lower bound of 6.6 TeV on the VEV of the SO(10) singlet that breaks the $U(1)_N$ symmetry at the TeV scale.

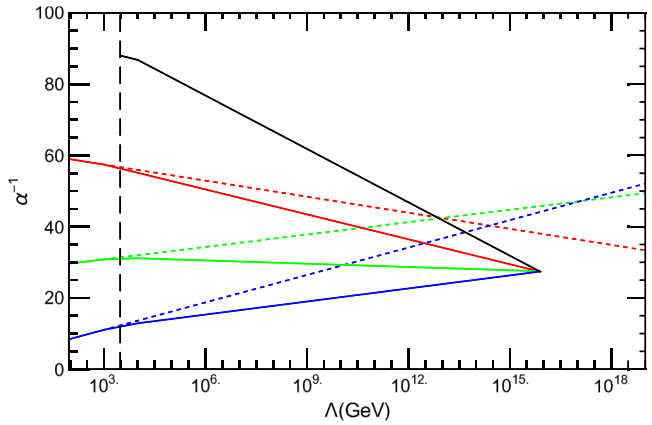

FIG. 10. RGE for the gauge couplings. Dashed lines: SM; solid lines: E_6 model with three 27-plet fermions + one 27-plet scalar + one 78-plet scalar + one 351′-plet scalar. Black (uppermost solid) curve, α_N^{-1} of $U(1)_N$; red (second from the top for solid, topmost for dashed at low energies) curve, α_1^{-1} of $U(1)_Y$; green (third from the top for solid, second from the top for dashed at low energies) curve, α_2^{-1} of $U(2)_L$; blue (third from the top for solid, third from the top for dashed at low energies) curve, α_3^{-1} of $U(3)_c$. The vertical line corresponds to the experimental lower bound on the Z_N mass.

The unification in Fig. 10 occurs at 8×10^{15} GeV, above the lower bound on the unification scale imposed by SuperKamiokande [113]. Thus as mentioned before all the additional particles that could facilitate proton decay can reside at this energy scale and the symmetry breaking from E_6 down to SM $\otimes$ $U(1)_N$ can occur at this scale via VEVs as described in Sec. II and Appendix A in a manner compatible with experiment. This demonstration of the unification is only at the one-loop level and with simplifications assumed in the evolution as mentioned above. Higher-order loops and threshold corrections will alter the scale at which unification occurs.

At the electroweak scale, the only constraint on the running coupling constant g_N is that of an upper bound coming from the precise measurement of the Higgs boson mass which prevents large mixing in the gauge boson mass matrix. If we change the high-energy constraint on g_N in Fig. 10 to demand unification, that will shift the topmost solid (black) line in the direction of higher α_N^{-1} values, thus further reducing the value of g_N at the electroweak scale which would be allowed by the Z mass constraints. Also, such an upward shift will always push the Landau pole to higher energies than the Planck-scale Landau pole case. Thus, g_N can always be unified with the other three coupling constants provided the other three have enough corrections due to the extra mass above the proton decay scale to enable their unification.

2. Yukawa and quartic couplings

The one-loop renormalization group equations for the Yukawa couplings in this model can be computed to give the following for the new Yukawa couplings [192,193] associated with the vectorlike quarks (y_D) and (y_L):

$$16\pi^2 \frac{dy_D}{dt} = y_D\left[\frac{9}{2}y_D^2 + 2y_L^2 - 8g_3^2 - \frac{2}{5}g_1^2 - \frac{39}{40}g_N^2\right], \tag{C6}$$

$$16\pi^2 \frac{dy_L}{dt} = y_L\left[3y_D^2 + \frac{7}{2}y_L^2 - \frac{9}{2}g_2^2 - \frac{9}{10}g_1^2 - \frac{39}{40}g_N^2\right], \tag{C7}$$

where $t = \ln(\Lambda/\mathrm{GeV})$. The computation can be simplified in the Landau gauge as noted in [192].

Figures 11 and 12 show the running of the Yukawa couplings when the g_N value at 3 TeV is set to be the one required by the one-loop unification as shown in Fig. 10. Thus this ensures unification as well as the Landau pole being higher than the Planck scale. The initial condition imposed for the running of the Yukawa coupling is $y_i(m_i) = \frac{m_i}{\langle\tilde{n}\rangle}$. For $\langle\tilde{n}\rangle = 1$ TeV, we show the evolution of couplings for $m_D = 950$ GeV and $m_L = 950$ GeV with electroweak value of 1.4 for b_{17} in Fig. 11 and for

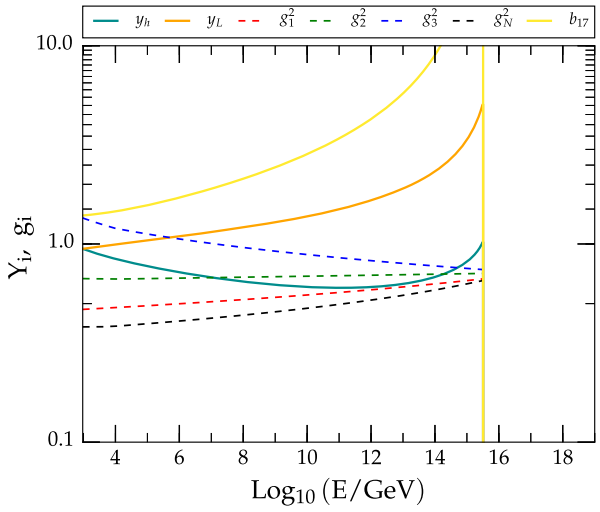

FIG. 11. RGE for the Yukawa couplings when g_N at MTeV scale is set to be the value required by unification. Dashed curves (upper to lower) correspond to g_3 (blue), g_2 (green), g_1 (red) and g_N (black). Solid curves (upper to lower) correspond to b_{17} (yellow), y_L (orange) and y_D (teal). Electroweak-scale Yukawa couplings are $y_D = 0.95$, $y_L = 0.95$ and quartic $b_{17} = 1.4$.

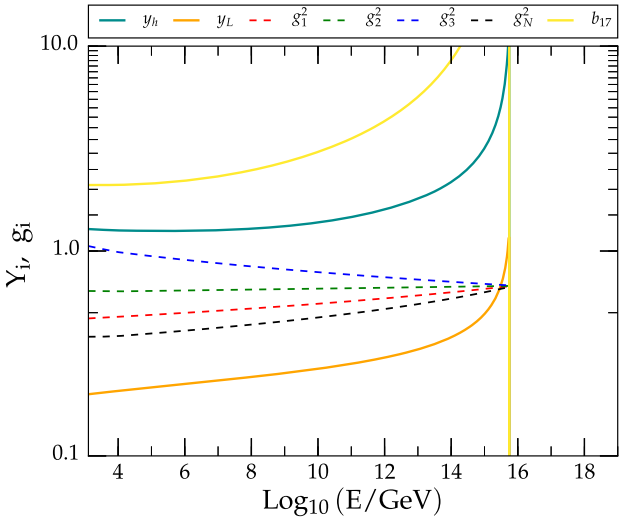

FIG. 12. RGE for the Yukawa couplings when g_N at MTeV scale is set to be the value required by unification. Dashed curves (upper to lower) correspond to g_3 (blue), g_2 (green), g_1 (red) and g_N (black). Solid curves (upper to lower) correspond to b_{17} (yellow), y_D (teal) and y_L (orange). Electroweak scale Yukawa couplings are $y_D = 1.3$, $y_L = 0.2$, $b_{17} = 2.1$.

$m_D = 1300$ GeV and $m_L = 200$ GeV with electroweak value of 2.1 for b_{17} in Fig. 12.

The values of the Yukawa couplings are chosen to demonstrate the maximum possible values under the condition $y_L = y_D$ (Fig. 11) and maximize the allowed y_D for the lowest m_L allowed by the experiments (Fig. 12). The LEP bounds on charged particle searches are ~100 GeV, while the stau searches at the LHC do not produce bounds stronger than 200 GeV [194,195]. Therefore, we are allowed to go as low as $y_L = 0.2$ for $\langle \tilde{n} \rangle = 1$ TeV to maximize the allowed y_D. As can be seen, any increase in the masses, i.e., Yukawa coupling values near the electroweak scale, will lead to Landau poles in Yukawa couplings below 10^{16} GeV.

Similarly reduction in values of the quartic coupling b_{17} will make the potential unstable below the GUT scale, and an increase in the electroweak scale value of b_{17} will lead to a Landau pole below the GUT scale. The difference between this maximum value of b_{17} allowed by one-loop perturbativity constraints and minimum value allowed by the stability constraint increases for smaller values of the Yukawa couplings as shown by the colored regions in the left panel of Fig. 9.

Finally, we note that owing to the large Q_N charges of $-5/\sqrt{40}$, $\pm 6/\sqrt{40}$ and $10/\sqrt{40}$, the low-energy degrees of freedom belonging to the $351'$-plet do not contribute to the Yukawa vertex at one-loop level and hence do not affect the Yukawa evolution at that level.

[1] H. Georgi and S. L. Glashow, Phys. Rev. Lett. **32**, 438 (1974).
[2] H. Georgi, AIP Conf. Proc. **23**, 575 (1975).
[3] H. Fritzsch and P. Minkowski, Ann. Phys. (N.Y.) **93**, 193 (1975).
[4] F. Gursey, P. Ramond, and P. Sikivie, Phys. Lett. **60B**, 177 (1976).
[5] P. Minkowski, Phys. Lett. **67B**, 421 (1977); M. Gell-Mann, P. Ramond, and R. Slansky, in *Supergravity*, edited by D. Freedman and P. Van Nieuwenhuizen (North-Holland, Amsterdam, 1979), pp. 315–321; T. Yanagida, Prog. Theor. Phys. **64**, 1103 (1980); R. N. Mohapatra and G. Senjanovic, Phys. Rev. Lett. **44**, 912 (1980).
[6] J. F. Gunion, H. E. Haber, G. L. Kane, and S. Dawson, *The Higgs Hunter's Guide*, (Perseus Books, New York, 1990); Reprinted in Front. Phys., **80**, 1 (2000).
[7] R. W. Robinett and J. L. Rosner, AIP Conf. Proc. **99**, 193 (2008).
[8] P. Langacker, R. W. Robinett, and J. L. Rosner, Phys. Rev. D **30**, 1470 (1984).
[9] D. London and J. L. Rosner, Phys. Rev. D **34**, 1530 (1986).
[10] J. L. Hewett and T. G. Rizzo, Phys. Rep. **183**, 193 (1989).
[11] J. L. Rosner, Phys. Rev. D **61**, 097303 (2000).
[12] T. C. Andre and J. L. Rosner, Phys. Rev. D **69**, 035009 (2004).

[13] J. D. Bjorken, S. Pakvasa, and S. F. Tuan, Phys. Rev. D **66**, 053008 (2002).
[14] J. L. Rosner, Comments Nucl. Part. Phys. **15**, 195 (1986).
[15] J. L. Rosner, Phys. Rev. D **90**, 035005 (2014).
[16] S. Nandi and U. Sarkar, Phys. Rev. Lett. **56**, 564 (1986).
[17] R. N. Mohapatra and J. W. F. Valle, Phys. Rev. D **34**, 1642 (1986).
[18] D. London, G. Belanger, and J. N. Ng, Phys. Rev. D **34**, 2867 (1986).
[19] M. Cvetic and P. Langacker, Phys. Rev. D **46**, R2759 (1992).
[20] E. Ma, Phys. Lett. B **380**, 286 (1996).
[21] Z. Chacko and R. N. Mohapatra, Phys. Rev. D **61**, 053002 (2000).
[22] M. Frank, I. Turan, and M. Sher, Phys. Rev. D **71**, 113001 (2005).
[23] M. Frank, I. Turan, and M. Sher, Phys. Rev. D **71**, 113002 (2005).
[24] P. S. Bhupal Dev and A. Pilaftsis, Phys. Rev. D **87**, 053007 (2013).
[25] S. J. Brice *et al.*, Fermilab report No. FERMILAB-FN-0947.
[26] J. M. Conrad, C. M. Ignarra, G. Karagiorgi, M. H. Shaevitz, and J. Spitz, Adv. High Energy Phys. 2013 (**2013**) 163897.
[27] M. Archidiacono, N. Fornengo, C. Giunti, S. Hannestad, and A. Melchiorri, Phys. Rev. D **87**, 125034 (2013).
[28] J. Kopp, P. A. N. Machado, M. Maltoni, and T. Schwetz, J. High Energy Phys. 05 (2013) 050.
[29] A. de Gouvea *et al.* (Intensity Frontier Neutrino Working Group Collaboration), arXiv:1310.4340.
[30] A. Aguilar-Arevalo *et al.* (LSND Collaboration), Phys. Rev. D **64**, 112007 (2001).
[31] A. A. Aguilar-Arevalo *et al.* (MiniBooNE Collaboration), Phys. Rev. Lett. **98**, 231801 (2007); **102**, 101802 (2009); **105**, 181801 (2010).
[32] G. Mention, M. Fechner, T. Lasserre, T. A. Mueller, D. Lhuillier, M. Cribier, and A. Letourneau, Phys. Rev. D **83**, 073006 (2011).
[33] T. A. Mueller *et al.*, Phys. Rev. C **83**, 054615 (2011).
[34] P. Huber, Phys. Rev. C **84**, 024617 (2011); **85**, 029901(E) (2012).
[35] See https://indico.cern.ch/event/442432/contribution/1/attachments/1205572/1759985/CERN-Seminar.pdf, LPCC seminar presented by Marumi Kado on behalf of the ATLAS Collaboration, CERN, 2015; ATLAS Collaboration, Report No. ATLAS-CONF-2015-081.
[36] ATLAS Collaboration, J. High Energy Phys. 09 (2016) 001.
[37] See https://indico.cern.ch/event/442432/contribution/0/attachments/1205563/1756687/CMS_13_TeV_results_public.pdf, LPCC seminar presented by Jim Olsen on behalf of the CMS Collaboration, CERN, 2015; CMS Collaboration, Report No. CMS PAS EXO-15-004.
[38] CMS Collaboration, Phys. Rev. Lett. **117**, 051802 (2016).
[39] ATLAS Collaboration, Report No. ATLAS-CONF-2016-059.
[40] ATLAS Collaboration, Report No. ATLAS-CONF-2017-059 (unpublished).
[41] CMS Collaboration, Phys. Lett. B **767**, 147 (2017).
[42] P. Ko, Y. Omura, and C. Yu, J. High Energy Phys. 04 (2016) 098.
[43] W. Chao, arXiv:1601.00633.
[44] A. Karozas, S. F. King, G. K. Leontaris, and A. K. Meadowcroft, Phys. Lett. B **757**, 73 (2016).
[45] C. Hati, Phys. Rev. D **93**, 075002 (2016).
[46] S. F. King and R. Nevzorov, J. High Energy Phys. 03 (2016) 139.
[47] G. C. Cho, N. Maru, and K. Yotsutani, Mod. Phys. Lett. A **31**, 1650130 (2016).
[48] P. Athron, M. Muhlleitner, R. Nevzorov, and A. G. Williams, J. High Energy Phys. 01 (2015) 153.
[49] G. K. Leontaris and Q. Shafi, Eur. Phys. J. C **76**, 574 (2016).
[50] Y. Cai, J. D. Clarke, R. R. Volkas, and T. T. Yanagida, Phys. Rev. D **94**, 033003 (2016).
[51] K. Das, T. Li, N. Nandi, and S. K. Rai, arXiv:1607.00810.
[52] D. Das, C. Hati, G. Kumar, and N. Mahajan, Phys. Rev. D **94**, 055034 (2016).
[53] A. E. Faraggi and J. Rizos, Eur. Phys. J. C **76**, 170 (2016).
[54] J. Ashfaque, L. Delle Rose, A. E. Faraggi, and C. Marzo, Eur. Phys. J. C **76**, 570 (2016).
[55] J. M. Ashfaque, arXiv:1607.03076.
[56] L. Delle Rose, A. E. Faraggi, C. Marzo, and J. Rizos, arXiv:1704.02579.
[57] S. F. King, S. Moretti, and R. Nevzorov, Phys. Rev. D **73**, 035009 (2006).
[58] S. F. King, S. Moretti, and R. Nevzorov, Phys. Lett. B **634**, 278 (2006).
[59] S. F. King, S. Moretti, and R. Nevzorov, Phys. Lett. B **650**, 57 (2007).
[60] R. Howl and S. F. King, J. High Energy Phys. 05 (2008) 008.
[61] S. F. King, R. Luo, D. J. Miller, and R. Nevzorov, J. High Energy Phys. 12 (2008) 042.
[62] P. Athron, S. F. King, D. J. Miller, S. Moretti, and R. Nevzorov, Phys. Lett. B **681**, 448 (2009).
[63] P. Athron, S. F. King, D. J. Miller, S. Moretti, and R. Nevzorov, Phys. Rev. D **80**, 035009 (2009).
[64] P. Athron, S. F. King, D. J. Miller, S. Moretti, and R. Nevzorov, AIP Conf. Proc. **1200**, 454 (2010).
[65] P. Athron, J. P. Hall, R. Howl, S. F. King, D. J. Miller, S. Moretti, and R. Nevzorov, Nucl. Phys. B, Proc. Suppl. **200–202**, 120 (2010).
[66] J. P. Hall, S. F. King, R. Nevzorov, S. Pakvasa, and M. Sher, Phys. Rev. D **83**, 075013 (2011).
[67] P. Athron, S. F. King, D. J. Miller, S. Moretti, and R. Nevzorov, Phys. Rev. D **84**, 055006 (2011).
[68] A. Belyaev, J. P. Hall, S. F. King, and P. Svantesson, Phys. Rev. D **86**, 031702 (2012).
[69] P. Athron, S. F. King, D. J. Miller, S. Moretti, and R. Nevzorov, Phys. Rev. D **86**, 095003 (2012).
[70] J. C. Callaghan and S. F. King, J. High Energy Phys. 04 (2013) 034.
[71] J. P. Hall, S. F. King, R. Nevzorov, S. Pakvasa, and M. Sher, AIP Conf. Proc. **1560**, 303 (2013).
[72] P. Athron, M. Binjonaid, and S. F. King, Phys. Rev. D **87**, 115023 (2013).

[73] P. Athron, D. Stockinger, and A. Voigt, Phys. Rev. D **86**, 095012 (2012).
[74] R. Nevzorov, Phys. Rev. D **87**, 015029 (2013).
[75] R. Nevzorov and S. Pakvasa, Phys. Lett. B **728**, 210 (2014).
[76] R. Nevzorov, Phys. Rev. D **89**, 055010 (2014).
[77] P. Athron, D. Harries, and A. G. Williams, Phys. Rev. D **91**, 115024 (2015).
[78] P. Athron, D. Harries, R. Nevzorov, and A. G. Williams, Phys. Lett. B **760**, 19 (2016).
[79] A. E. Faraggi and J. Rizos, Nucl. Phys. **B895**, 233 (2015).
[80] R. Franceschini, G. F. Giudice, J. F. Kamenik, M. McCullough, A. Pomarol, R. Rattazzi, M. Redi, F. Riva, A. Strumia, and R. Torre, J. High Energy Phys. 03 (2016) 144.
[81] R. S. Gupta, S. Jager, Y. Kats, G. Perez, and E. Stamou, J. High Energy Phys. 07 (2016) 145.
[82] W. Altmannshofer, J. Galloway, S. Gori, A. L. Kagan, A. Martin, and J. Zupan, Phys. Rev. D **93**, 095015 (2016).
[83] A. Djouadi, J. Ellis, R. Godbole, and J. Quevillon, J. High Energy Phys. 03 (2016) 205.
[84] F. Staub *et al.*, Eur. Phys. J. C **76**, 516 (2016).
[85] R. Franceschini, G. F. Giudice, J. F. Kamenik, M. McCullough, F. Riva, A. Strumia, and R. Torre, J. High Energy Phys. 07 (2016) 150.
[86] M. Bauer and M. Neubert, Phys. Rev. D **93**, 115030 (2016).
[87] P. S. B. Dev, R. N. Mohapatra, and Y. Zhang, J. High Energy Phys. 02 (2016) 186.
[88] E. Palti, Nucl. Phys. **B907**, 597 (2016).
[89] T. Li, J. A. Maxin, V. E. Mayes, and D. V. Nanopoulos, J. High Energy Phys. 06 (2016) 167.
[90] J. Jiang, T. Li, and D. V. Nanopoulos, Nucl. Phys. **B772**, 49 (2007).
[91] M. E. Peskin and T. Takeuchi, Phys. Rev. Lett. **65**, 964 (1990).
[92] M. E. Peskin and T. Takeuchi, Phys. Rev. D **46**, 381 (1992).
[93] A. Joglekar, P. Schwaller, and C. E. M. Wagner, J. High Energy Phys. 12 (2012) 064.
[94] R. W. Robinett and J. L. Rosner, Phys. Rev. D **26**, 2396 (1982).
[95] S. F. Mantilla, R. Martinez, F. Ochoa, and C. F. Sierra, Nucl. Phys. **B911**, 338 (2016).
[96] B. Dutta, Y. Gao, T. Ghosh, I. Gogoladze, T. Li, and J. W. Walker, Phys. Rev. D **94**, 036006 (2016).
[97] E. Witten, Nucl. Phys. **B258**, 75 (1985).
[98] P. Candelas, G. T. Horowitz, A. Strominger, and E. Witten, Nucl. Phys. **B258**, 46 (1985).
[99] J. D. Breit, B. A. Ovrut, and G. C. Segre, Phys. Lett. B **158**, 33 (1985).
[100] M. Dine, V. Kaplunovsky, M. L. Mangano, C. Nappi, and N. Seiberg, Nucl. Phys. **B259**, 549 (1985).
[101] R. Slansky, in *Recent Developments in High Energy Physics: Proceedings,* edited by A. Perlmutter and L. F. Scott (Plenum Press, New York, 1980), p. 141.
[102] T. Matsuoka, H. Mino, D. Suematsu, and S. Watanabe, Prog. Theor. Phys. **76**, 915 (1986).
[103] L. E. Ibanez and J. Mas, Nucl. Phys. **B286**, 107 (1987).
[104] S. F. King, S. Moretti, and R. Nevzorov, Phys. Rev. D **73**, 035009 (2006); Phys. Lett. B **634**, 278 (2006).
[105] R. Slansky, Phys. Rep. **79**, 1 (1981).
[106] J. Schwichtenberg, arXiv:1704.04219.
[107] CMS Collaboration, Phys. Lett. B **720**, 63 (2013).
[108] ATLAS Collaboration, Phys. Rev. D **90**, 052005 (2014).
[109] ATLAS Collaboration, ATLAS Report No. ATLAS-CONF-2016-045, 2016.
[110] CMS Collaboration, CMS Report No. CMS PAS EXO-16-031, 2016.
[111] R. Radogna, on behalf of ATLAS and CMS Collaborations, in Proceedings of 52nd Rencontres de Moriond EW 2017, La Thuile, Italy (unpublished).
[112] ATLAS Collaboration, Report No. ATLAS-CONF-2017-027, 2017.
[113] K. Abe *et al.* (Super-Kamiokande Collaboration), Phys. Rev. D **95**, 012004 (2017).
[114] J. M. Arnold, B. Fornal, and M. B. Wise, Phys. Rev. D **87**, 075004 (2013).
[115] CMS Collaboration, Phys. Rev. D **93**, 032005 (2016); **95**, 039906(E) (2017).
[116] CMS Collaboration, arXiv:1703.03995.
[117] ATLAS Collaboration, New J. Phys. **18**, 093016 (2016).
[118] P. Cox, A. Kusenko, O. Sumensari, and T. T. Yanagida, J. High Energy Phys. 03 (2017) 035.
[119] CMS Collaboration, Phys. Lett. B **747**, 98 (2015).
[120] S. Dimopoulos and H. Georgi, in *Proceedings of the Second Workshop on Grand Unification, University of Michigan, Ann Arbor, 1981*, edited by J. P. Leveille, L. R. Sulak, and D. G. Unger (Birkhauser, Boston, 1981), pp. 285–296.
[121] L. Randall and C. Csaki, in *Proceedings of International Workshop on Supersymmetry and Unification of Fundamental Interactions (SUSY 95), Palaiseau, France, 1995*, edited by I. Antoniadis and H. Videau (Edition Frontières, Gif-sur-Yvette, 1996), pp. 99–109.
[122] G. R. Dvali, Phys. Lett. B **372**, 113 (1996).
[123] A. Falkowski, O. Slone, and T. Volansky, J. High Energy Phys. 02 (2016) 152.
[124] A. Falkowski, Pramana **87**, 39 (2016).
[125] CMS Collaboration, Phys. Rev. D **93**, 112009 (2016).
[126] ATLAS Collaboration, Phys. Rev. D **91**, 112011 (2015).
[127] N. Craig, P. Draper, C. Kilic, and S. Thomas, Phys. Rev. D **93**, 115023 (2016).
[128] I. Low and J. Lykken, arXiv:1512.09089.
[129] J. F. Kamenik, B. R. Safdi, Y. Soreq, and J. Zupan, J. High Energy Phys. 07 (2016) 042.
[130] C. Csaki and L. Randall, J. High Energy Phys. 07 (2016) 061.
[131] ATLAS Collaboration, ATLAS Report No. ATLAS-CONF-2015-075, 2015.
[132] CMS Collaboration, Report No. CMS PAS EXO-16-019.
[133] M. Bauer, M. Neubert, and A. Thamm, arXiv:1607.01016.
[134] S. I. Godunov, A. N. Rozanov, M. I. Vysotsky, and E. V. Zhemchugov, JETP Lett. **103**, 557 (2016).
[135] C. Csaki, J. Hubisz, and J. Terning, Phys. Rev. D **93**, 035002 (2016).
[136] S. Fichet, G. von Gersdorff, and C. Royon, Phys. Rev. D **93**, 075031 (2016).
[137] S. Fichet, G. von Gersdorff, and C. Royon, Phys. Rev. Lett. **116**, 231801 (2016).

[138] C. Csaki, J. Hubisz, S. Lombardo, and J. Terning, Phys. Rev. D **93**, 095020 (2016).
[139] K. Ghosh, S. Jana, and S. Nandi, arXiv:1607.01910.
[140] S. K. Agarwalla, K. Ghosh, and A. Patra, arXiv:1607.03878.
[141] M. K. Sundaresan and P. J. S. Watson, Phys. Rev. Lett. **29**, 15 (1972); L. Resnick, M. K. Sundaresan, and P. J. S. Watson, Phys. Rev. D **8**, 172 (1973).
[142] J. R. Ellis, M. K. Gaillard, and D. V. Nanopoulos, Nucl. Phys. **B106**, 292 (1976).
[143] A. Djouadi, Phys. Rep. **457**, 1 (2008); **459**, 1 (2008).
[144] M. Low, A. Tesi, and L. T. Wang, J. High Energy Phys. 03 (2016) 108.
[145] S. Dulat, T.-J.Hou, J. Gao, M. Guzzi, J. Huston, P. Nadolsky, J. Pumplin, C. Schmidt, D. Stump, and C. P. Yuan, Phys. Rev. D **93**, 033006 (2016).
[146] ATLAS Collaboration, Eur. Phys. J. C **75**, 510 (2015); **76**, 153(E) (2016).
[147] ATLAS Collaboration, Phys. Lett. B **760**, 647 (2016).
[148] ATLAS Collaboration, Report No. ATLAS-CONF-2017-015 (unpublished).
[149] ATLAS Collaboration, Report No. ATLAS-CONF-2017-022 (unpublished).
[150] CMS Collaboration, J. High Energy Phys. 06 (2015) 116.
[151] CMS Collaboration, Report No. CMS-PAS-SUS-17-001 (unpublished).
[152] CMS Collaboration, Report No. CMS-PAS-SUS-16-008 (unpublished).
[153] CMS Collaboration, Report No. CMS-PAS-SUS-16-032 (unpublished).
[154] CMS Collaboration, Report No. CMS-PAS-SUS-16-051 (unpublished).
[155] J. Kawamura and Y. Omura, Phys. Rev. D **93**, 115011 (2016).
[156] M. Carena, P. Huang, A. Ismail, I. Low, N. R. Shah, and C. E. M. Wagner, Phys. Rev. D **94**, 115001 (2016).
[157] ATLAS Collaboration, Phys. Rev. D **88**, 112003 (2013).
[158] ATLAS Collaboration, J. High Energy Phys. 01 (2015) 068.
[159] ATLAS Collaboration, Phys. Lett. B **760**, 647 (2016).
[160] CMS Collaboration, J. High Energy Phys. 07 (2013) 122.
[161] CMS Collaboration, Report No. CMS-PAS-EXO-15-010.
[162] CMS Collaboration, J. High Energy Phys. 01 (2015) 096.
[163] CMS Collaboration, Eur. Phys. J. C **75**, 151 (2015).
[164] ATLAS Collaboration, J. High Energy Phys. 11 (2014) 104.
[165] ATLAS Collaboration, J. High Energy Phys. 08 (2015) 105.
[166] CMS Collaboration, Phys. Rev. D **93**, 012003 (2016).
[167] J. L. Rosner, Phys. Rev. D **35**, 2244 (1987).
[168] See https://launchpad.net/mg5amcnlo.
[169] Benjamin Fuks (private communication to ATLAS and CMS Collaborations), tabulated at https://twiki.cern.ch/twiki/bin/view/LHCPhysics/SUSYCrossSections.
[170] ATLAS Collaboration, New J. Phys. **15**, 093011 (2013).
[171] ATLAS Collaboration, J. High Energy Phys. 09 (2015) 108.
[172] ATLAS Collaboration, Phys. Rev. D **92**, 032001 (2015).
[173] S. Grancagnolo, on behalf of the ATLAS Collaboration, *Proc. Sci.*, EPS-HEP2015 (2015) 096.
[174] ATLAS Collaboration, New J. Phys. **18**, 073021 (2016).
[175] CMS Collaboration, Phys. Lett. B **718**, 348 (2012).
[176] CMS Collaboration, Phys. Rev. D **90**, 032006 (2014).
[177] CMS Collaboration, Report No. CMS-PAS-EXO-14-001.
[178] CMS Collaboration, J. High Energy Phys. 03 (2016) 125.
[179] CMS Collaboration, Report No. CMS PAS EXO-16-002.
[180] S. Dodelson and L. M. Widrow, Phys. Rev. Lett. **72**, 17 (1994).
[181] X.-D. Shi and G. M. Fuller, Phys. Rev. Lett. **82**, 2832 (1999).
[182] A. Kusenko, Phys. Rep. **481**, 1 (2009).
[183] K. N. Abazajian *et al.*, arXiv:1204.5379.
[184] E. Bulbul, M. Markevitch, A. Foster, R. K. Smith, M. Loewenstein, and S. W. Randall, Astrophys. J. **789**, 13 (2014).
[185] A. Boyarsky, O. Ruchayskiy, D. Iakubovskyi, and J. Franse, Phys. Rev. Lett. **113**, 251301 (2014).
[186] M. Drewes *et al.*, J. Cosmol. Astropart. Phys. 01 (2017) 025.
[187] M. Carena, A. Daleo, B. A. Dobrescu, and T. M. P. Tait, Phys. Rev. D **70**, 093009 (2004).
[188] E. Accomando, A. Belyaev, L. Fedeli, S. F. King, and C. Shepherd-Themistocleous, Phys. Rev. D **83**, 075012 (2011).
[189] J. L. Rosner, Phys. Lett. B **221**, 85 (1989).
[190] J. L. Rosner, Phys. Rev. D **54**, 1078 (1996).
[191] D. J. Gross and F. Wilczek, Phys. Rev. Lett. **30**, 1343 (1973).
[192] T. P. Cheng, E. Eichten, and L. F. Li, Phys. Rev. D **9**, 2259 (1974).
[193] E. Ma and S. Pakvasa, Phys. Rev. D **20**, 2899 (1979).
[194] ATLAS Collaboration, J. High Energy Phys. 05 (2014) 071.
[195] CMS Collaboration, Eur. Phys. J. C **74**, 3036 (2014).